Modeling and Upscaling of Shale Gas Using a Discrete Fracture Modeling Approach

MSc Thesis

Tarek Awadalla

TUDelft

TU Delft

DELFT UNIVERSITY OF TECHNOLOGY

MASTER THESIS

Modeling and Upscaling of Shale Gas Using a Discrete Fracture Modeling Approach

Author:
Tarek AWADALLA

Supervisor:
Dr. Denis VOSKOV

A thesis submitted in fulfillment of the requirements for the degree of Master of Science

in the

Department of Geosciences and Engineering
Petroleum Engineering Section

February 27, 2017

Author

Tarek Awadalla
T.Awadalla@student.tudelft.nl
MSc Student, Petroleum Engineering & Geosciences
Department of Geoscience and Engineering
Delft University of Technology

Advisor

Dr. Denis Voskov
D.V.Voskov@tudelft.nl
Associate Professor
Department of Geoscience and Engineering
Delft University of Technology

Commitee

Dr. Hadi Hajibeygi
H.Hajibeygi@tudelft.nl
Assistant Professor
Department of Geoscience and Engineering
Delft University of Technology

Dr. Paul van Hoek
P.J.vandenHoek@tudelft.nl
Senior Research Associate
Department of Geoscience and Engineering
Delft University of Technology

Prof. Dr. Giovanni Bertotti
G.Bertotti@tudelft.nl
Head of Section
Department of Geoscience and Engineering
Delft University of Technology

An electronic version of this dissertation is available at
http://repository.tudelft.nl/.

Delft University of Technology

Abstract

Faculty of Civil Engineering and Geosciences
Department of Geosciences and Engineering

Master of Science

Modeling and Upscaling of Shale Gas Using a Discrete Fracture Modeling Approach

by Tarek AWADALLA

Gas flow in fractured nano-porous shale formations is complicated by a hierarchy of structural features, ranging from nanopores to microseismic and hydraulic fractures, and by several transport mechanisms that differ from standard viscous flow used in reservoir modelling. In small pores, self-diffusion becomes more important than advection, also slippage effect and Knudsen diffusion becomes relevant at this scale.

The characteristics and properties of the fracture networks plays a major role in the performance of shale gas reservoirs, therefore the use of accurate simulation technique that honor the complexity of these reservoirs and capture the associated dynamics of nanopores is strongly required. However, these accurate simulations often necessitate a large amount of computations for field scale models and therefore require upscaling. Yet the upscalling techniques generally in use are based on idealizations that do not reflect the discrete features of the reservoir.

In this work, we first incorporate the formulations of a statistical bundle of dual tube model to describe the dynamics of shale gas into a discrete fracture model. The formulation of the DFM model we use applies an unstructured control volume finite difference approach with a two point flux approximation. We then propose to upscale these detailed descriptions using two different techniques, with the major difference in their coarse grid geometry. The first approach, referred to as EDFM upscaling, relies on a structured Cartesian coarse grid. While the second method, which we call the multiple subregion (MSR) upscaling, introduces a flow based coarse grid to replicate the diffusive character of the pressure in the matrix. The required parameters for the coarse scale model in both methods and the geometry of the subregions in the second method are determined efficiently from global single-phase flow solution using the underlying discrete fracture model.

The methods are applied to simulate single-phase gas flow in 2D fractured reservoir models, and are shown to provide results in close agreement with the underlying DFM and with considerable reduction in the computational time. We notice that in order to account for the prevailing transient effects in low permeability shale, the upscaled transmissibility need to be related to pressure for better results.

Finally, we consider the EDFM upscaling we propose as an easier approach in its implementation, while the MSR technique as a more accurate method.

Acknowledgements

My extreme gratitude goes to my adviser Dr. Denis Voskov for giving me the opportunity to work with him and for his continuous support. Over the course of this research I have benefited a lot from his knowledge, advice and encouragement.

I am also very thankful to the support I have received from Mark Khait, for the time he has dedicated into helping me especially in the early times of my work.

I would like to acknowledge the Stanford University Petroleum Research Institute for Reservoir Simulation (SUPRI-B) program for the permission to use ADGPRS in this work.

Finally, I would like to thank my family; partner, parents and friends who had supported and encouraged me all the time during my studies.

Contents

List of Figures

List of Tables

List of Abbreviations

ADGPRS	**A**utomatic **D**ifferentiation **G**eneral **P**urpose **R**esearch **S**imulator
BHP	**B**ottom **H**ole **P**ressure
BoDTM	**B**undle **o**f **D**ual **T**ubes **M**odel
BoTM	**B**undle **o**f **T**ubes **M**odel
DFM	**D**iscrete **F**racture **M**odel
EDFM	**E**mbedded **D**iscrete **F**racture **M**odel
EIA	**E**nergy **I**nformation **A**dministration
FEM	**F**inite **E**lement **M**ethod
FVM	**F**inite **V**olume **M**ethod
MSR	**M**ultiple **S**ub **R**egions
PeBi	**Pe**rpendicular **Bi**sector
PI	**P**roductivity **I**ndex
REV	**R**epresentative **E**lementary **V**olume
TPFA	**T**wo **P**oint **F**lux **A**pproximation

List of Symbols

α	Half transmissibility	
δ	Molecular diameter	m
κ	Dimensionless constant	[-]
μ	Viscosity	cp
ϕ	Porosity	[-]
ρ	Density	kg/m^3
σ	Cross-sectional area of collision	m^2
σ_v	Tangential-momentum accommodation	[-]
ξ	Numerical prefactor	[-]
A	Area	m^2
d	Pore throat diameter	m
D	Distance	m
D^m	Molecular diffusion coefficient	m^2/s
D^k	Knudsen diffusion coefficient	m^2/s
D_{eff}	Effective diffusion coefficient	m^2/s
$\vec{f}$	Unit vector	[-]
h	Fracture aperture	m
k	Permeability	$darcies$
k_B	Boltzmann constant	JK^{-1}
K_N	Knudsen number	[-]
l	Gas mean free path	m
m	Molecular mass	kg
$\vec{n}$	Unit normal vector	[-]
p	Pressure	$bars$
PV	Pore Volume	m^3
q	Mass flow rate	kg/d
R	Universal gas constant	$m^3 bar K^{-1} mol^{-1}$
T	Temperature	K
t	Time	d
T_A	Advective flux transmissibility	
T_D	Diffusive flux tranmissibility	
u	Mean gas velocity	m/d
V	Volume	m^3
v_T	Thermal velocity	m/s

Chapter 1

Introduction and literature review

Within the hydrocarbon family, the fastest growing hydrocarbon resource is natural gas. Natural gas is becoming the primary source of electricity generation for many nations around the world, its popularity is due to its reduced greenhouse gas emissions compared to other fossil fuels.

The emergence of shale gas resources largely increases global natural gas reserves. The U.S Energy Information Administration (EIA) estimates that known shale gas deposits worldwide add 47 percent to the global technically recoverable natural gas resources Fig.1.1. However, extracting the gas from shale poses a number of risks to the environment that needs to be accounted for in order to benefit from the potential resources previously recognized as economically infeasible owing to their low productivity.

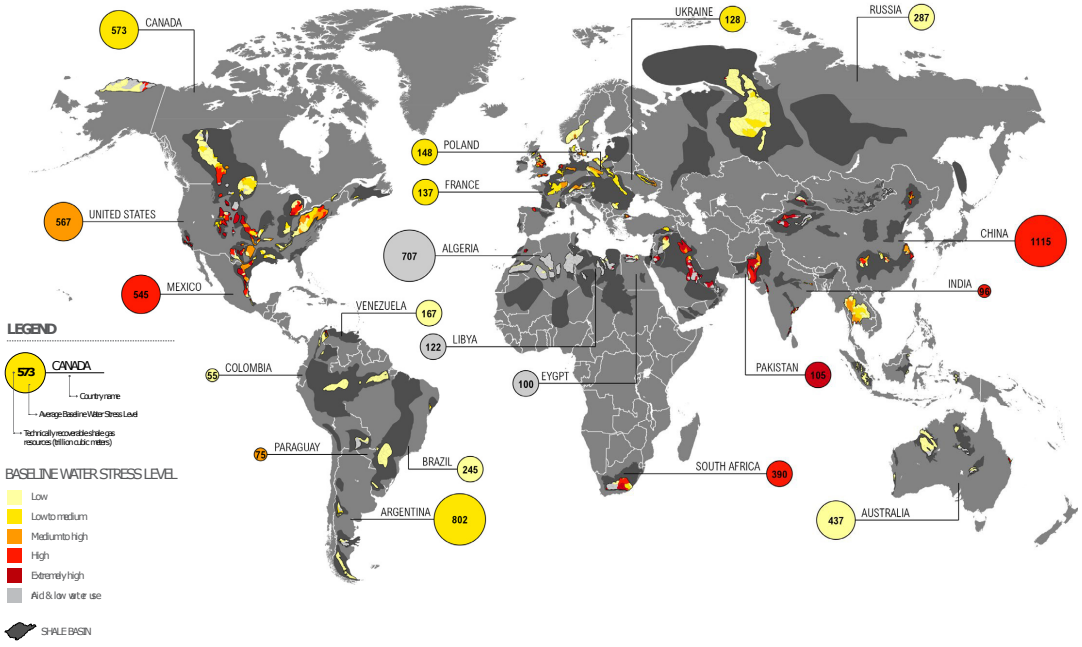

FIGURE 1.1: Location of world's shale play and the volume of technically recoverable shale gas [1] [2]

As shale gas reservoirs are characterized by a very low permeability, gas production can only be achieved by stimulating the shale formation through hydraulic fracturing. Combined with horizontal drilling it maximises extraction by allowing multiple fractures along the shale bed which in turn allows the gas to be commercially

[1] Source: World resources institute

[2] The map is also intended to show the level of baseline water stress which is outside the scope of this research

extracted. The large development costs of shale gas reservoirs makes it a necessity to develop accurate and reliable modelling tools for uncertainty quantification and risks assessment.[1]

The use of conventional reservoir simulation methods cannot provide reasonable production analysis for shale gas reservoirs because they are designed for viscous displacement processes (Hadjiconstantinou, 2006). These tools strongly underestimate the potential of shale gas resources due to the highly nonlinear and complex mechanisms driving the flow in extremely low permeability formations.

Researchers (e.g. Javadpour et al., 2007; Darabi et al., 2012) recently characterized complex networks of nanopores within shale gas which behave differently than Darcy flow. They identified that the gas release in shale is the outcome of several different transport mechanisms, mainly viscous flow and molecular diffusion induced by gas expansion. Additionally, the no-slip boundary condition is no longer adequate as pore diameter become within the order of the molecular mean free path, which also induces molecule-wall collisions and affects the diffusion coefficient (Knudsen effect). Hence, it is necessary to account for the different dynamics in shale gas, which are normally not considered in traditional reservoir simulations.

Furthermore, the analysis of gas production from shale formation is complicated by a hierarchy of structural features induced by the multistage hydraulic fracturing and the consequent micro-seismic events which creates a connected network of secondary fractures within the reservoir.

The characteristics of the generated fracture systems are crucial to estimate shale gas production rate, yet their geometrical complexity along the strong permeability contrast between fractures and nano-pores of shale is a challenge for reservoir simulation.

Next we will introduce several models for simulation of flow in fractured media.

1.1 Fracture modeling methods

1.1.1 Discrete fracture model (DFM)

In DFM approach each fracture is modelled explicitly using, in most of the cases, highly resolved unstructured grids. This allowed the simulation of fine scale geological models with complex and various fracture geometries. For these reasons, DFM is considered as the most accurate representation of fracture networks but with the disadvantage of high computational cost as a tremendous amount of grid cells are involved.

Various procedures to solve the flow equations for systems using unstructured grids can be found in the literature. Using finite element approach such as the earliest work of Baca et al. (1984) as they proposed to solve for 2D single-phase flow with heat and solute transport. Juanes et al. (2002) presented a more general approach with finite-element formulation for 2D and 3D for single-phase flow in fractured porous media. These early methods were then extended to handle incompressible two-phase fluid flow including capillary pressure effect such as in the work of

[1] Data and information about natural gas, shale gas resources and its development were gathered from various resources on the web such as:

- EIA: https://www.eia.gov/
- Shale Gas Europe: http://shalegas-europe.eu/
- Resources for the Future: http://www.rff.org/

Kim and Deo (2000) and Karimi-Fard and Firoozabadi (2001), compositional multi-component flow in Hoteit and Firoozabadi (2005), and three-phase flow in Fu et al. (2005).

Matthäi et al. (2005) presented a control-volume finite-element (CVFE) approach to accurately quantify two-phase flow simulation in fractured rock masses using 3D hybrid meshes. Their work was then expanded to include applications for compressible three phase flow in Matthäi et al. (2007) and in Geiger-Boschung et al. (2009).

Finite element procedures are generally more expensive than the standard finite-volume, the latter being most popular choice among the majority of existing reservoir simulation techniques. Karimi-Fard et al. (2003) offered a simplified DFM based on a finite volume approach. The method is applicable to connection list based general purpose reservoir simulators and offers significant improvement in the efficiency of DFM's using unstructured grids.

There are, however, some effective procedures based on structured discretization schemes. For example, Lee et al. (2001) presented a hierarchical modelling of flow in fractured formations. In this model, the small fractures were introduced by adjusting the reservoir properties, while the large fractures were modelled explicitly. Another proposed method also using structured grids is the embedded discrete fracture model (EDFM: Li and Lee, 2008), in which the fractures are discretized separately from the matrix and then coupled together using a transfer term.

It is only the advances in geological characterization tools as well as the improved computational capabilities that allowed implementation of DFMs for modelling complex fracture networks.

1.1.2 Dual continuum models

One of the most popular and practical flow model applied in fractured reservoir is the dual-porosity model. The idea, introduced by Barenblatt and Zheltov (1960), is founded on the subdivision of the system into two separate continuum, where matrix represent most of fluid storage while large-scale flow occurs through the fractures. The exchange of flow between matrix and fracture is represented by a transfer function. Warren and Root (1963) proposed an idealized representation of the reservoir using a set of identical rectangular parallelepipeds as matrix blocks, separated by fractures Fig.1.2. In their approach, flow takes place only through the fracture network while the matrix blocks are feeding the fractures though a transfer function.

The transfer function, also known as the shape-factor, has been the subject of many investigation. This parameter generally depends on the shape of the matrix block and the flow mechanisms.

Interblock matrix-matrix flow is not represented in the dual-porosity model.
Blaskovich et al. (1983) and Hill and Thomas (1985) introduced the dual-porosity/dual-permeability models where matrix to matrix connections were considered to account for the contribution of matrix to the overall flow.

This addition allowed to improve the capabilities of dual continuum models, which was limited to highly connected fractured reservoir, in simulating variations of fracture network densities.

Despite being a computationally attractive approach, the dual-continuum models are too limited to represent detailed geological characterization. In such cases, discrete fracture modelling offers the required accuracy.

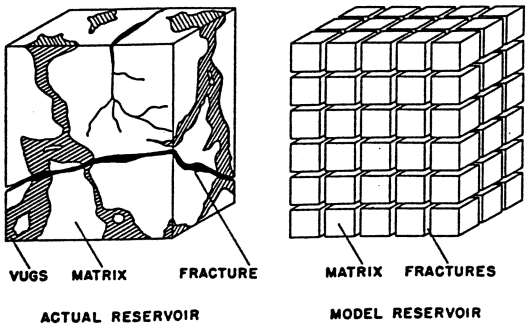

FIGURE 1.2: Idealized dual-porosity reservoir model (Warren and Root, 1963)

1.2 Upscaling

The detailed geological description of highly heterogeneous fractured reservoirs are generally far too fine for direct flow simulation and therefore need to be upscaled. Sablok and Aziz (2008) summarizes upscaling errors in reservoir simulation. They focused on the errors introduced by local single-phase upscaling, for any type of heterogeneous reservoirs, as a result of coarsening and homogenization.

The conventional dual continuum models (dual-porosity (Barenblatt and Zheltov, 1960), dual-porosity/dual-permeabiltiy (Blaskovich et al., 1983; Hill and Thomas, 1985)) are the mostly widely used representation for upscaling fractured reservoir. As mentioned in the previous section, in the dual porosity model, the matrix acts as source that feeds the fractures and flow occurs only in fractures. This limitation was corrected for with the dual-porosity/dual-permeability procedure. In these models, equivalent permeability for the coarse block is determined through local single phase flow simulations over the fine scale model. The major limitation brought by using these models, in addition to the fracture network idealization, is the assumption of an existing REV. Such assumption is generally accepted in formations with highly interconnected dense fracture network but is not applicable for poorly connected networks or if the network fractures has no characteristic size limit (Berkowitz, 2002).

Lee et al. (2001) proposed a hierarchical fracture upscaling that is meant to reduce the error brought by homogenization when fracture length scale distribution is non-uniform or the network is poorly connected. In their approach, large scale fractures were modeled explicitly and the effective permeability contribution from smaller fractures was determined analytically.

The EDFM model in Li and Lee (2008) can also be used for upscaling of fractured networks. This method, represents an interesting development to the dual continuum approaches, where fracture networks are discretely connected to matrix blocks by a series of source terms. It also has the advantage that fractures and matrix are represented by independent grid domains. However, difficulties might arises when evaluating the transfer function to describe exchange of fluid between matrix and fracture.

In an effort to tackle limitation of conventional upscaling approaches, Vitel and Souche (2007) proposed a technique based on the upscaling of transmissibility from a fine scale "pipe network". The workflow involve a simplification stage where nodes are removed iteratively by applying electric simplifications then it is followed by an optimization step where connections of low transmissibility are removed. This approach is rather appealing as it does not depend on computing effective properties.

Recently, Gong et al. (2006) and Karimi-Fard et al. (2006) presented a systematic multi-subregion (MSR) upscaling approach based on the integration of DFM into a general multiple continuum representation. The method was developed as an effort to include spatial variability within local matrix region, considering that most of the dual-porosity implementations model the pressure and saturation as constant within the matrix. They succeed to resolve spatial variation within the matrix with a novel flow-based subgridding technique using the solution of a local discrete fracture flow problem over each coarse grid block. The parameters for the coarse scale model are also extracted from the solution of DFM fine scale flow problems. Application of the method to simulate 2D and 3D fracture models, with viscous, gravitational and capillary pressure effect is also shown in their work.

1.3 Research objectives

In shale gas, we are mostly dealing with a single phase problem; which despite being considered as the simplest form of upscaling, the transient phenomena associated to the low permeability of shale formation as well as its complex setting brought by the complex fracture networks represent a challenge to standard upscaling methods.

In this research, our goal is to benefit from the accuracy of discrete fracture representation to model shale gas dynamics in fractured environment. We also would like to develop an upscaling procedure with the capacity to approximately reproduce the same flow behaviour as the original DFM solution in shale gas.

To achieve our objectives, we propose two upscaling models with a systematic workflow, and analyse their applicability on fractured shale gas. The methods we study here are based on adaptation and modifications to the EDFM method and the multi subregion method (MSR) in order to include formulation describing the shale gas dynamics and provide accurate upscaled results.

1.4 Flow simulation

We perform all of our simulations using the Stanford automatic differentiation general purpose research simulator (ADGPRS) developed by Voskov et al. (2009). ADGPRS is a unified reservoir simulation framework providing an extensive set of nonlinear formulations (Voskov and Tchelepi, 2011; Voskov, 2012; Zaydullin et al., 2012), flexible spatial discretization (Zhou et al., 2011), and implements a connection list approach where each grid node may have a variable and arbitrary number of neighbouring or connected nodes that depends on the grid geometry. In such implementation, there is no distinct dimensionality as the conventional spatial indices i,j,k are not used but rather a unique number is assigned to each block.

The specification of all possible pairs of connections are established in an array during discretization performed at a preprocessing stage. Note that for no flow boundaries the connections are excluded.
Such implementation has the advantage to simplify redundant flux calculations that may occur in conventional block based approach, as inter-block fluxes are only evaluated when pairs of grid blocks are connected.

This thesis proceeds as follows, in chapter 2 the different transport physics in shale gas and their equations are described. Chapter 3 presents the DFM approach we are implementing to describe shale gas dynamics in fractured formation with example application. Then the proposed upscaling procedures and their application are explained in chapter 4, with analysis of the upscaled results. Finally, the thesis conclusions are presented in chapter 5.

Chapter 2

Gas Dynamics in Shale

To investigate the dynamics of gas flow in complex shale systems we had recourse to a conceptual model. Conceptual models are a representation of the systems, with the sole objective to convey fundamental principles and functionality of the represented process which help to improve the understanding of the phenomena.

Pore network geometries are in general very complex; various conceptual models were previously proposed and successfully used to model flow in porous media (Fig.2.1). The complexity of the model in literature varies from simple bundle of tubes (Fatt, 1956), throat-bulb model (Lee et al., 1996) and the more complex pore network reconstruction using 3D imaging tools (Blunt et al., 2013). The degree of complexity of the relevant network should reflect the complexity of the physical phenomena to be described.

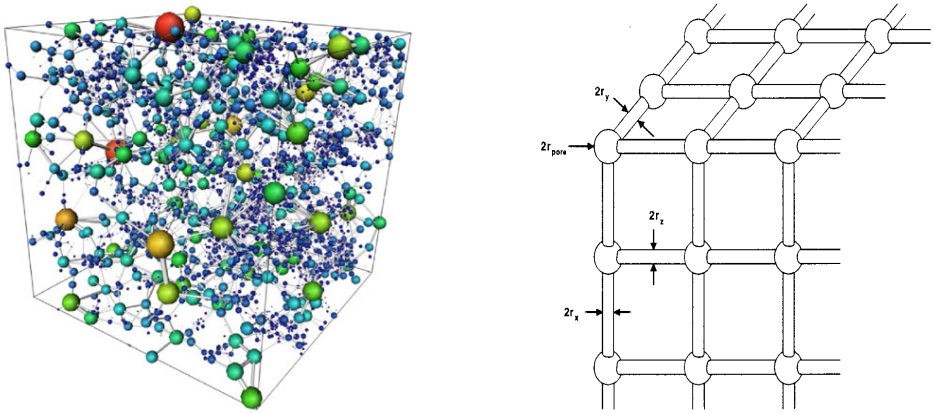

(A) (B)

FIGURE 2.1: Porous network conceptual models, (A) Pore network extracted from 3D imaging tools (Blunt et al., 2013) (B) bulb throat model (Lee et al., 1996)

Owing to the fact that we are concerned by the modeling of single phase gas, a simplified model can be used. In this research, we adapt the formulation of a bundle of dual tube model (Lunati and Lee, 2014) in a numerical framework to represent the pore network structure in shale gas and capture the relevant macroscopic effects. Considering the fact that most of the matrix storage volume is provided by pores connected through their pore throats, Lunati and Lee proposed a statistical BoDtm as a generalization of the BoTM, where the effect of the successive pores and throats is homogenized. Hence, each pathway is described by two effective diameters; a large diameter describes the effective storage along the tube and a smaller diameter which represent the effective permeability of the throats Fig.2.2.

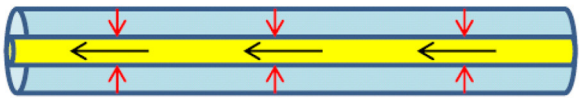

FIGURE 2.2: A dual tube conceptual model (Lunati and Lee, 2014)

In our adaptation, which is numerical rather than statistical, the matrix storage is represented by the pore volume of the corresponding control volume (discretized element of the reservoir) while the flow across neighboring control volumes is controlled by the effective permeability of a bundle of tubes. Our concern, is to model the dynamics of shale gas with respect to the complex settings brought by the networks of fractures generally characterized in shale formations.

2.1 Physics of gas transport in shale formation

Gas flow in low permeability shale gas cannot be modeled using standard Darcy flow models designed for viscous dominated displacement. As the size of the confining pore space reduces to nano-scale, the validity of the standard approach based on Navier-Stokes equation with no-slip boundary condition diminishes (Hadjiconstantinou, 2006) see the Fig.2.3.

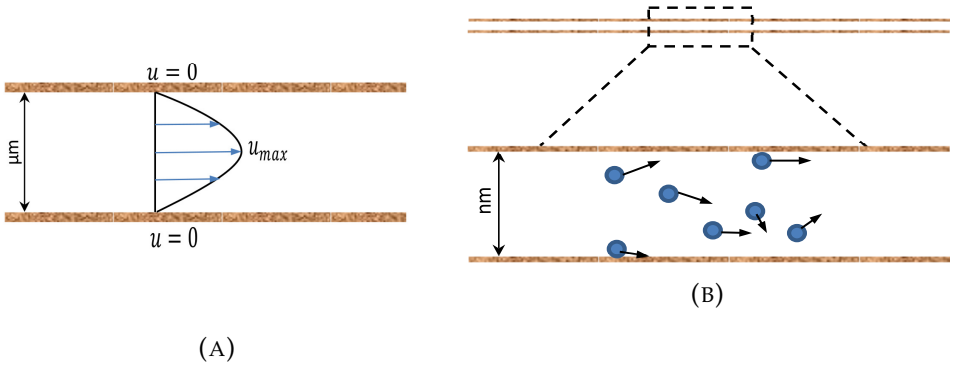

FIGURE 2.3: (A) no-slip flow in micro scale pores and (B) slip flow in nano size pores

Researchers (e.g. Javadpour et al., 2007; Darabi et al., 2012 as well as others) identified the main transport mechanisms in shale gas as viscous flow and self-diffusion due to gas expansion. Additionally, as pore diameter become of the order of the molecular mean free path the molecule-wall collisions becomes more pronounced, also known as Knudsen effect. Therefore, it is necessary to account for these different flow regimes to model gas flow in shale formations.

Knudsen number, K_N, is used in order to determines the appropriateness of the continuum model, Fig. 2.4. It is a widely recognized dimensionless parameter, defined as the ratio of the gas mean free path l and the pore diameter d,

$$K_N = \frac{l}{d}, \tag{2.1}$$

where l the molecular mean free path is defined as the average distance the molecules of gas travels between two successive collisions with other molecules. Using kinetic

elementary theory, and assuming a Maxwell-Boltzmann distribution of the velocity, the mean free path becomes:

$$l = \left(\frac{m}{\sqrt{2}\sigma}\right)\frac{1}{\rho}, \tag{2.2}$$

in which m is the molecular mass and σ is the cross-sectional area of collision. For methane $\sigma = \pi\delta^2 = 0.42\ nm^2$, using a methane molecular diameter $\delta = 3.8°A$.

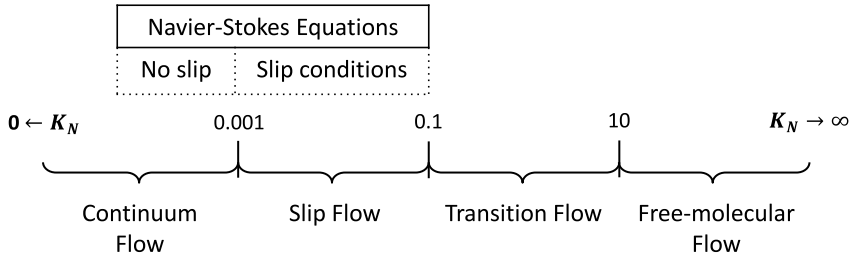

FIGURE 2.4: Flow regime classification based on Knudsen number

2.1.1 General mass balance

The study of transport phenomenon in general entails the analysis of conservation of mass within the system. The general mass balance equation that is used to describe the flow through porous medium, for an element (control volume) within the medium is defined as:

$$\frac{\partial(\phi\rho)}{\partial t} + \nabla.j = q. \tag{2.3}$$

The equation depicts the accumulation of mass, the mass flux through the system and the physio-chemical reactions respectively, where ρ is the density, ϕ is the porosity, j is the total flux and q is the source term.

The total flux refers to the dominating physical processes. In the modeling process, this is an advective flux due to mean gas velocity and a diffusive flux due to density gradient,

$$j = j_{adv} + j_{diff} = u\rho - D\frac{\partial\rho}{\partial x}. \tag{2.4}$$

The diffusive flux is related to density gradient using the diffusion coefficient D, while the mean gas velocity is defined as proportional to pressure gradient using Darcy's law as follow:

$$u = -\frac{k}{\mu}\frac{\partial p}{\partial x}, \tag{2.5}$$

where k is the absolute permeability tensor and μ is the viscosity of the gas.

The analysis of the gas kinetics that governs the physics of gas inside the pores investigated by Lunati and Lee is presented next. Lunati and Lee based their results on elementary kinetic theory for an isothermal system, suggesting that the low porosity of shale and the small gas flux besides the large thermal capacity and conductivity of the rock leads to negligible effects on temperature.

2.1.2 Permeability with slip effect correction

Based on the Hagen–Poiseuille equation for viscous flow in a pipe, permeability in the longitudinal direction can be expressed as:

$$k = \kappa d^2, \tag{2.6}$$

where κ is a dimensionless constant that is related to the configuration of the flow-paths ($1/32$ for a circular tube and $1/12$ for planar fractures), d is the diameter of the circular tube or the aperture of a plane fracture.

As pore size d becomes very small and comparable to the mean free path l, the no-slip condition at the solid boundary is no more applicable and the equation has to be modified. Brown et al. (1946) proposed a correction to account for the slippage effect as:

$$k = \left[1 + 4\frac{l}{d}\left(\frac{2}{\sigma_v} - 1\right)\right]\kappa d^2, \tag{2.7}$$

where κ is the same dimensionless constant as in equation 2.6, $0 < \sigma_v < 1$ is the tangential-momentum accommodation coefficient that indicates the fraction of molecules that are diffusively reflected by the wall. Assuming we have tubes of rough surfaces that reflects all molecules diffusively, then $\sigma_v = 1$ and substituting with the definition of mean free path in Eq.2.2, the equation simplifies to:

$$k = \left[1 + 4\frac{m}{\sqrt{2}\sigma\rho d}\right]\kappa d^2. \tag{2.8}$$

2.1.3 Viscosity

The viscosity defines the ability of intermolecular collisions to transfer momentum and based on the elementary kinetic theory of gases (Hirschfelder et al., 1954), it is defined as:

$$\mu = \frac{1}{3}\rho l v_t, \tag{2.9}$$

where v_T, the thermal velocity, is interpreted as the mean magnitude of the molecular velocity and is given by:

$$v_T = \sqrt{\frac{8k_B}{\pi m}}T^{\frac{1}{2}}, \tag{2.10}$$

where $k_B = 1.38$ x $10^{-23} JK^{-1}$ is the Boltzmann constant.

Therefore μ can be written as:

$$\mu = \xi_\mu \frac{\sqrt{k_B m/\pi}}{\sigma} T^{\frac{1}{2}}, \tag{2.11}$$

where the numerical prefactor $\xi_\mu = 2/3$.

Note that viscosity is only a function of temperature; hence it is considered as constant for isothermal processes.

2.1.4 Molecular diffusion coefficient

The molecular diffusion coefficient describes the mass transfer due to molecular collisions, and therefore is proportional to the thermal velocity and to the mean free path:

$$D^m = \frac{1}{3} l v_T. \tag{2.12}$$

The molecular diffusion coefficient then becomes:

$$D^m = \xi_D \frac{\sqrt{k_B m/\pi}}{\sigma} \frac{T^{\frac{1}{2}}}{\rho}, \tag{2.13}$$

with $\xi_D = 2/3$.
The equation above is used to describe self-diffusion for a pure gas.

2.1.5 Knudsen diffusion

When the size of the pore d is comparable to or smaller than the mean free path of the gas molecules l, the interactions with the solid walls of the pores become more significant than the intermolecular interactions. The mass transfer due to the effects of collision with the wall is described by the Knudsen diffusion coefficient, obtained by replacing l by d in equation 2.12:

$$D^k = \frac{1}{3} d v_T = D^m \frac{d}{l}. \tag{2.14}$$

2.1.6 Effective diffusion

The Knudsen number is also used to describe the relative importance of the molecule-molecule collisions with respect to the molecule-wall collisions, which varies depending on the reservoir conditions. Knudsen diffusion is more likely to be prevailing at lower pressure, while molecular diffusion in nano-pores is dominant at higher pressure as intermolecular collisions are more likely. To consider the contribution of these two mechanisms, the effective diffusion coefficient introduced by Lunati and Lee is used:

$$D_{eff} = D^m \left[1 + K_N\right]^{-1}, \tag{2.15}$$

which describes their combined effect and tends to D^m when $K_N << 1$ and to D^k when $K_N >> 1$.

2.1.7 Adsorption and desorption

In shale gas, the gas is stored as compressed gas in pores but also as adsorbed gas to the pore walls and as soluble gas in solid organic materials (Javadpour et al., 2007). As the pressure within the reservoir is depleted by production, the adsorbed gas gets released into the nano-pores followed by the diffusion of organic matter dissolved gas to the surface of the pores.

The volume of adsorbed gas in shale formations can be of large quantities; up till now its significance to production is the subject of many studies and analyses of different types of shales (e.g. Yu and Sepehrnoori, 2014; Yang et al., 2015, and the references therein), and its contribution is mostly accounted at the very low pressures of late stage recovery.

For simplicity we will only include the contribution of free gas trapped in the rock pores into our simulations.

2.2 Flow in fractures

Fractures are generally characterized with a much higher permeability than the shale matrix despite the different fractures categorized within shale formations. The Knudsen number for the flow of gas in these fractures mostly fall below 0.001, which indicate a viscous dominated flow.

The simplest model of flow through a rock fracture is the parallel plate model (Sarkar et al., 2004), where fracture walls are represented by parallel plates separated by an aperture "h". This model provide exact same solution as Navier-Stokes and therefore can be formulated in the same way as Darcy's law. The average velocity within a fracture is then given by:

$$u = -\frac{h^2}{12\mu}\frac{\partial p}{\partial x}, \tag{2.16}$$

where $\frac{h^2}{12}$ is basically the fracture permeability.

Chapter 3

Fracture Modeling

The economical profitability of shale formation came to significance with emergence of the improved recovery techniques by means of long horizontal wells stimulated by multi-staged hydraulic fracturing treatment.
The hydraulic fractures and the micro-seismic events following the stimulation process allow the well to communicate with the shale reservoir, creating a complex network of multiple length scale fractures.
The characteristics and properties of these fracture networks play an important role in shale gas reservoir performance. Therefore, it is significantly important to accurately characterize and represent these features in the modeling of these formations.

In this chapter, the approach used to model fractured shale gas is clarified. The numerical formulation of the equations used and adapted into the reservoir simulator are also explained, along with several test cases to show the dynamics of gas flow in fractured shale.

3.1 Discrete fracture modelling DFM

Discrete fracture models, in which the fractures are represented individually, are considered as one of the most accurate techniques to model fracture networks. However, DFM approaches are sought to require rigorous computations. Recently, improved techniques and advances in numerical solution methods have significantly improved its efficiency.

In this work, we follow the approach proposed by Karimi-Fard et al. (2003) where an unstructured control volume finite-difference technique with a two point flux approximation is used.

3.1.1 Geometrical discretisation

The first step covers the partitioning of the reservoir domain into discrete control volumes where the conservation law is locally applied.
To accurately capture the complexity of the fracture network, it is usually necessary to use an unstructured discretization scheme. The use of unstructured grids allow the modelling of non-ideal fracture geometries, such as non-orthogonal and non-planar fracture orientations.
In this work we employ a standard Delaunay triangulation scheme (TRIANGLE) Shewchuk (1996) to discretize the domain. For a 2D problem, the matrix blocks are represented by polygons while fractures are represented by segments.

The fracture thickness is not represented in the grid domain but only in the computational domain for flow rate evaluation, which consequently simplifies the gridding of fractured domain as showin in Fig. 3.1.

The mean properties of the grid block as well as the evaluated variables are defined in nodes, at the centroid of each corresponding control volume which is representative of the entire grid block.

Various unstructured gridding schemes can be used in a similar fashion; R. Schneiders listed on his webpage many of the meshing tools we can found online : http://www.robertschneiders.de/meshgeneration/software.html.

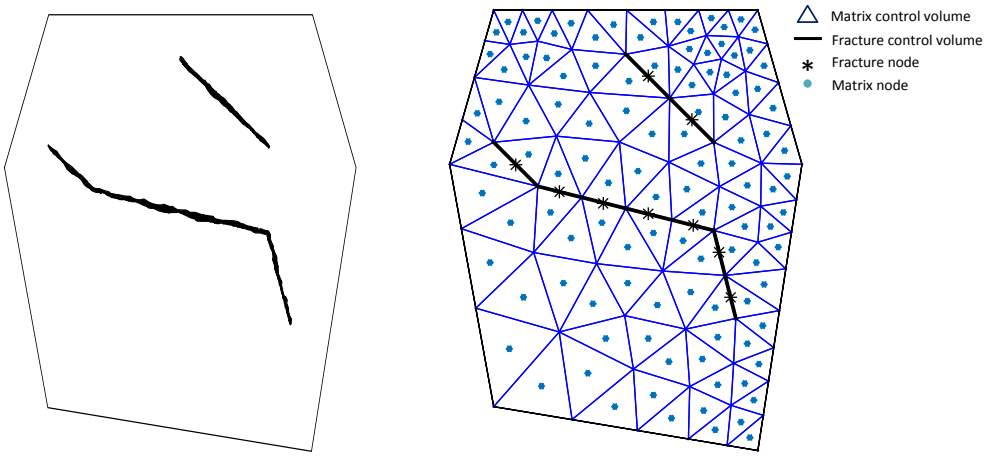

FIGURE 3.1: (A) 2D fracture domain, (B) Discretization using unstructured triangulation

One can notice that our discretization scheme generate grids that are not necessarily orthogonal, unlike the Perpendicular Bisector (PEBI) grids which are orthogonal by construction but introduce a lot of small control volumes. This issue with generally unstructured grids can be improved by simple modifications to the discretization as summarized in the work of Karimi-Fard (2008).

3.1.2 Numerical formulation

The mass balance equation for single phase, single component shale system after substituting with all the derived coefficients corresponding to each of the transport physics in shale gas as explained in chapter 2 will be:

$$\frac{\partial(\phi\rho)}{\partial t} = \nabla.\left[\phi\frac{\rho}{\mu}\left(1+4K_N\right)\kappa d^2.\nabla p + \phi\frac{D^m}{1+K_N}.\nabla\rho\right] + q. \tag{3.1}$$

The left hand side represents the temporal accumulation of mass, whereas the right hand side depicts the mass flow rate of the gas by convection and diffusion plus the source/sink term. Notice that porosity (ϕ) was introduced to the flux term to reform it for porous media.

Integration of the partial differential equation, over a finite control volume, ΔV, gives:

$$\frac{\partial}{\partial t}\iiint_{\Delta V}(\phi\rho)dV = \iiint_{\Delta V}\nabla.\left[\phi\frac{\rho}{\mu}\left(1+4K_N\right)\kappa d^2.\nabla p + \phi\frac{D^m}{1+K_N}.\nabla\rho\right]dV + \iiint_{\Delta V} q\,dV. \tag{3.2}$$

Applying the Gauss divergence theorem, the volume integral on the mass flux term can be rewritten as:

$$\iiint_{\Delta V} \nabla.\left[\phi\frac{\rho}{\mu}\left(1+4K_N\right)\kappa d^2.\nabla p+\phi\frac{D^m}{1+K_N}.\nabla\rho\right]dV = \iint_{\Delta A}\left[\phi\frac{\rho}{\mu}\left(1+4K_N\right)\kappa d^2.\nabla p+\phi\frac{D^m}{1+K_N}.\nabla\rho\right].\vec{n}\,dA, \quad (3.3)$$

where $\vec{n}$ is the outward unit vector of the surface ΔA and $\iint_{\Delta A}$ is the surface integral over the boundary of the control volume.

The source/sink is assumed to be uniformly distributed over the control volume, therefore:

$$\iiint_{\Delta V} q\,dV = Q. \quad (3.4)$$

Finally, the integrated mass balance becomes:

$$\frac{\partial}{\partial t}\iiint_{\Delta V}(\phi\rho)dV = \iint_{\Delta A}\left[\phi\frac{\rho}{\mu}\left(1+4K_N\right)\kappa d^2.\nabla p+\phi\frac{D^m}{1+K_N}.\nabla\rho\right].\vec{n}\,dA+Q. \quad (3.5)$$

3.1.3 Discretization of the mass balance equation

After we defined the flow equation in its integral form, the next steps is to discretize it using control volume finite difference approach with a cell-centered scheme. In this method the fluxes across control volume faces are defined in terms of the pressures only in the two cells sharing each of the interfaces, also known as a two-point flux approximation (TPFA).

For a given gridblock i, the volume integral of the accumulation term is approximated to:

$$\frac{\partial}{\partial t}\iiint_{\Delta V}(\phi\rho)dV = \frac{\partial}{\partial t}\left[(\phi\rho)_i V_i\right], \quad (3.6)$$

and its finite difference form is:

$$\frac{\partial}{\partial t}\left[(\phi\rho)_i V_i\right] = \frac{PV_i}{\Delta t}(\rho^{n+1}-\rho^n), \quad (3.7)$$

where $PV_i = (\phi V)_i$ is the pore volume of gridblock i, n is the time step level and Δt is the time step length.

To approximate the surface integral of the flux term in eq.(3.5), we subdivide the surface A_i into subsurface A_{ij} for N neighboring blocks in order to represent the individual boundaries between the reference block i and each of its neighbors:

$$A_i = \sum_{j=1}^{N} A_{ij}. \quad (3.8)$$

Consequently, the surface integral in eq.(3.5) can be interpreted as the summation of the fluxes across each interface of the grid block i to its neighbors j:

$$\iint_{\Delta A} \left[\phi\frac{\rho}{\mu}\left(1+4K_N\right)\kappa d^2.\nabla p+\phi\frac{D^m}{1+K_N}.\nabla\rho\right].\vec{n}\,dA = \sum_{j=1}^{N}\iint_{A_{ij}} \left[\phi\frac{\rho}{\mu}\left(1+4K_N\right)\kappa d^2.\nabla p+\phi\frac{D^m}{1+K_N}.\nabla\rho\right].\vec{n}\,dA. \quad (3.9)$$

The integral in (3.9) is then approximated and represented in the its finite difference form as:

$$\iint_{A_{ij}} \left[\phi\frac{\rho}{\mu}\left(1+4K_N\right)\kappa d^2.\nabla p+\phi\frac{D^m}{1+K_N}.\nabla\rho\right].\vec{n}\,dA = \sum_{j=1}^{N} A_{ij}\left[\phi\frac{\rho}{\mu}\left(1+4K_N\right)\kappa d^2.\frac{(p_j-p_i)}{D_{ij}}+\phi\frac{D^m}{1+K_N}.\frac{(\rho_j-\rho_i)}{D_{ij}}\right].\vec{n}. \quad (3.10)$$

The discretized form of the flow equation can finally be written as:

$$\frac{PV_i}{\Delta t}(\rho^{n+1}-\rho^n) = \sum_{j=1}^{N} A_{ij}\left[\phi\frac{\rho}{\mu}\left(1+4K_N\right)\kappa d^2.\frac{(p_j-p_i)}{D_{ij}}+\phi\frac{D^m}{1+K_N}.\frac{(\rho_j-\rho_i)}{D_{ij}}\right]^{n+1}.\vec{n} + Q_i^{n+1}. \quad (3.11)$$

3.1.4 Transmissibility

The discretized flow term can be represented in terms of a list of connected control volumes, where flow rate is related to pressure gradient by a transmissibility term. For each control volume (V), we express the flow rate across each one of its interfaces with the neighbouring cells as:

$$Q_{ij} = \phi[\lambda T_A + T_D](p_j - p_i), \quad (3.12)$$

which depicts the flow rate from V_i to V_j.

Notice that we use two transmissibility terms to account for the coefficients corresponding to the advective flux and diffusive flux, T_A and T_D respectively
The terms λ is the ratio $\frac{\rho}{\mu}$ and along with the porosity ϕ, they are both computed using upstream information (upwind)[1].

The transmissibilities are defined at the interface using a harmonic average of the properties within the connected blocks in a similar fashion as done for corner-point systems Ponting (1989).
In general, the harmonic average of tranmissibility is computed as:

$$T_{ij} = \frac{\alpha_i\alpha_j}{\alpha_i+\alpha_j}. \quad (3.13)$$

As said we defined two different T_ij, for each of which the term α will be:

[1] we relate density to pressure using the equation of state for an ideal gas $\rho = \frac{pm}{RT}$, where R is the universal gas constant and is equal to 8.31446 x $10^{-5} m^3 bar K^{-1} mol^{-1}$

- for advection

$$\alpha_i = \frac{A_{ij}}{D_i}(1 + 4K_N)\kappa d^2 \, \vec{n_i}.\vec{f_i}, \tag{3.14}$$

- for diffusion

$$\alpha_i = \frac{A_{ij}}{D_i}\frac{D^m}{(1 + K_N)}\frac{m}{RT} \, \vec{n_i}.\vec{f_i}, \tag{3.15}$$

while α_j for both transmissibilities is computed in the exact same manner but using the corresponding subscript j.

In 3.14 and 3.15 A_{ij} is the area of the interface between the neighboring V_i and V_j, D_i is the distance between the centroid of the interface and the centroid of V_i, $\vec{n_i}$ is the unit normal to the interface inside V_i and $\vec{f_i}$ is the unit vector along the direction of the line joining the control volume centroid to the centroid of the interface as illustrated in Fig. 3.2.The dot product of these two unit vectors $\vec{n_i}$ and $\vec{f_i}$ is simply equivalent to $\cos(\theta)$, where θ represents the angle between these two vectors. Note that for a 2D problem the interface is represented by a segment.

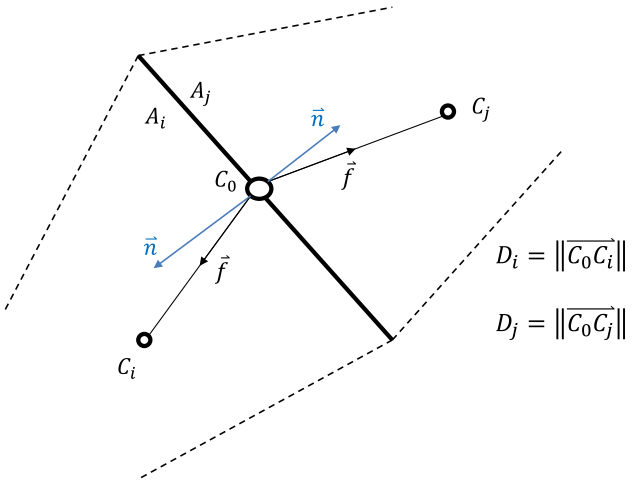

FIGURE 3.2: Geometrical representation of adjacent control volumes and the parameters included in transmissibility computation

3.1.5 Fracture transmissibility

The transmissibility for a connection between two fractures in a 2D problem is computed similarly , owing to a simplification proposed by Karimi-Fard et al. (2003). They propose to implicitly account for an intermediate control volume (V_0) to redirect the flow between the two segments as shown in Fig.3.3.

The use of this intermediate volume in the way proposed allows the modelling of fractures with varying thickness without the need to estimate unknowns at the introduced cell, which prevent any numerical complication. The simplification is based on the fact that such intermediate control volume will typically have similar properties to the adjacent cells and has a much smaller volume.

Therefore, equation 3.13 is used to compute fracture-fracture transmissibility, but here the term α is defined differently, since the flow is only dominated by viscous forces as explained in section 2.2. In that case there is only a single transmissibility term (purely geometrical) and α will simply be:

$$\alpha_i = \frac{A_i}{D_i}\kappa h_i^2, \tag{3.16}$$

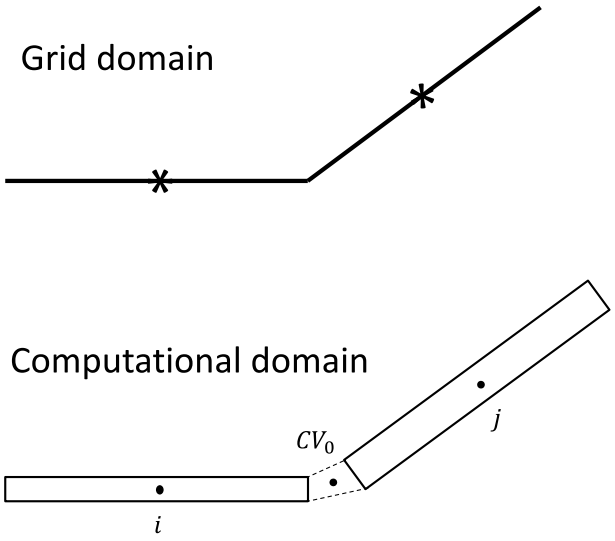

FIGURE 3.3: Connection between two fracture segments with an intermediate control volume used for flow computation only

where $\kappa = \frac{1}{12}$ and h_i is the fracture aperture of the i-th block, we note that $\vec{n}_i.\vec{f}_i$ is equal to 1 in such configuration and α_j is formulated similarly with properties of the j-th block.

3.1.6 Multiple intersections

The application of "star-delta" transformation for a network of resistors used in electrical circuits, has found popularity in simplifying the transmissibility computation for a system of fractures intersecting at a point. The analogy is quite useful especially when it comes to more than 2 fracture segments meeting at a point.

In Fig. 3.4 we show an example of fractures intersecting at a point. For such network the transmissibility is computed using:

$$\begin{aligned} T_{12} &= \frac{\alpha_1\alpha_2}{\alpha_1+\alpha_2+\alpha_3+\alpha_4}, \; T_{13} = \frac{\alpha_1\alpha_3}{\alpha_1+\alpha_2+\alpha_3+\alpha_4}, \\ T_{14} &= \frac{\alpha_1\alpha_4}{\alpha_1+\alpha_2+\alpha_3+\alpha_4}, \; T_{23} = \frac{\alpha_1\alpha_2}{\alpha_1+\alpha_2+\alpha_3+\alpha_4}, \\ T_{24} &= \frac{\alpha_2\alpha_4}{\alpha_1+\alpha_2+\alpha_3+\alpha_4}. \end{aligned} \tag{3.17}$$

Therefore for an intersection with n connections, Eq.3.17 can be generalized to:

$$T_{ij} \simeq \frac{\alpha_i\alpha_j}{\sum_{k=1}^{n}\alpha_k}. \tag{3.18}$$

3.2 Flow simulations

To show the applicability of the discrete fracture model, presented in our work, to model the dynamics of gas flow in fractured shale we present the results of flow simulations performed with ADGPRS. The problems modeled here represent the pressure solution for a fractured reservoir with its fracture network connected to a producing well. We model only the pressure profile of the reservoir over time,

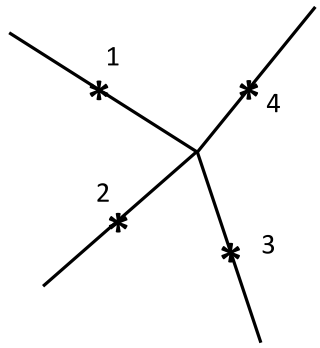

FIGURE 3.4: multiple fracture segments intersected at a point represented in the grid domain

since the dynamics of reservoir pressure depletion in shale gas represents the most important factor in their development strategies.

3.2.1 Simple fractured porous media

In this example, simulations are performed over a simple configuration of intersected fractures, all connected, in a 100 x 100 m^2 domain as shown in Fig.3.5. The porosity of the matrix is 6% while its permeability is defined by a pore throat diameter of 1 nano-meter ($10^{-9}m$). The fractures has an aperture of 1 mm ($k_{frac} = 84.1md$). The initial reservoir pressure and temperature are 200 bars and 423 degK (150 $°C$) respectively, and the well is producing by a controlled bottom hole pressure of 100 bar. The domain is bounded by a no-flux boundary.

The geometry is discretized using a Delaunay triangulation shown in Fig.3.6 with approximately 5000 triangles.

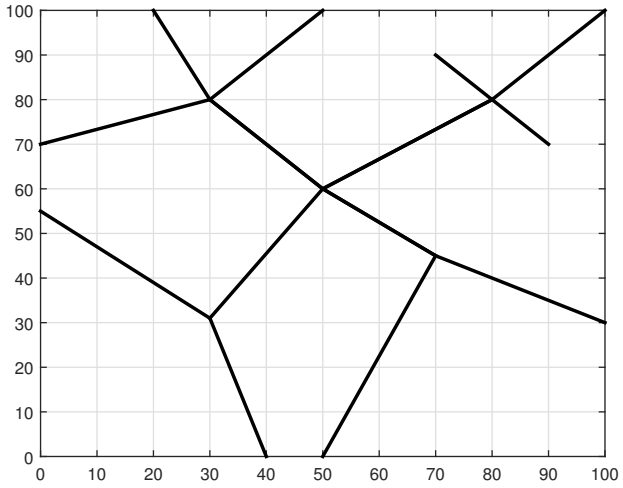

FIGURE 3.5: Simple fractured medium

Fig.3.7a represents the pressure profile after 1000 days of gas production, the different transport mechanisms related to flow in shale media are taken into account in the model while Fig.3.7b depicts the same simulation based on a basic Darcy flow model where only viscous flow is introduced.

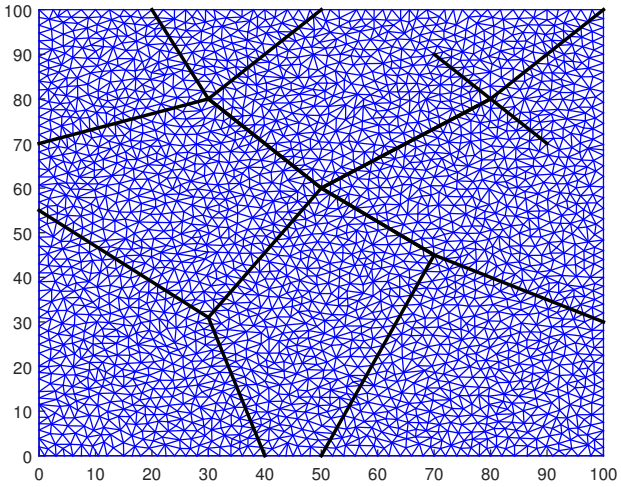

FIGURE 3.6: Delaunay triangulation of the simple fracture medium

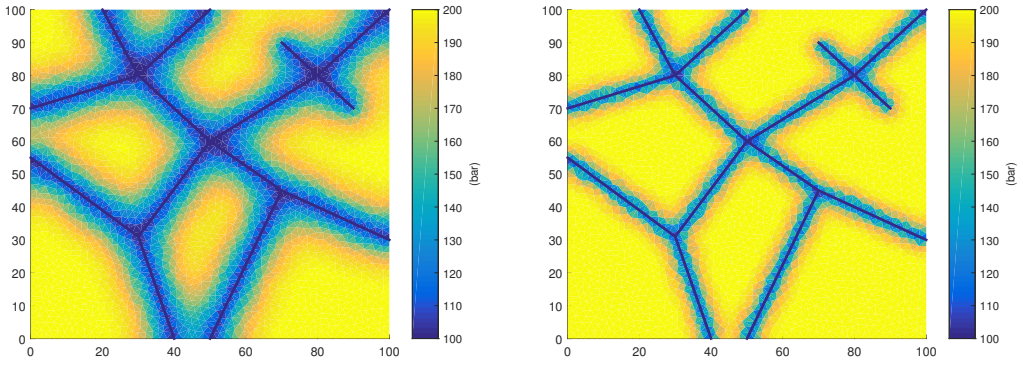

(A) (B)

FIGURE 3.7: Pressure profile at 1000 day of production (A) using shale gas model and (B) using Darcy model

These simulations are repeated at a higher permeability ($d = 10^{-7}m$), as shown in Fig.3.8, indicating that both model becomes similar at higher permeability when viscous flow is the dominant regime.

3.2.2 Complex fractured network

In this example we show the applicability of the presented model on a larger scale complex fracture network with realistic geological features obtained from Boersma (2016) and shown in Fig.3.9, where the majority of the represented fractures are connected with each other at their intersections. The model is simulated using similar initial conditions as used for the low permeability fracture network shown in the previous example. The domain has a dimension of 5.5 km (width) and 7 km (length), discretized with about 16,000 control volume.

The simulation is performed using the shale gas model, assuming the fractured network is connected to a well producing for about 50,000 days as shown in Fig.3.10. Due to the larger spacial scale, the transient effects are more significant in this mode in comparison to the previous example.

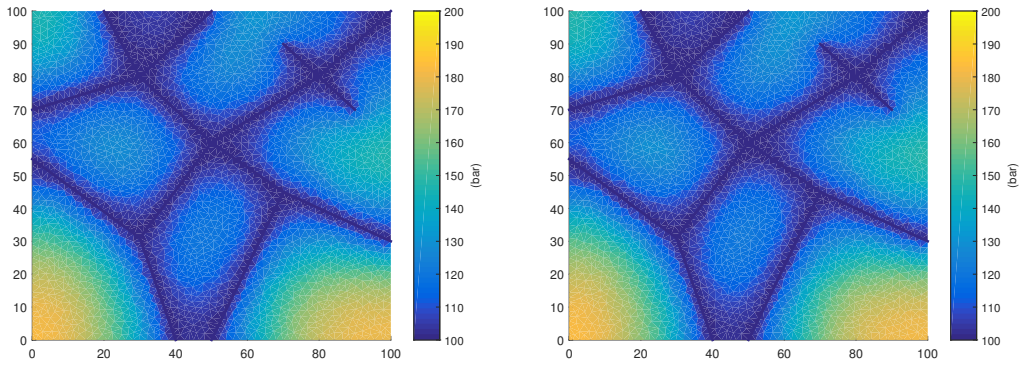

(A) (B)

FIGURE 3.8: Flow simulation at higher permeability ($d = 10^{-7}m$) (A) Shale model, (B) Darcy model.

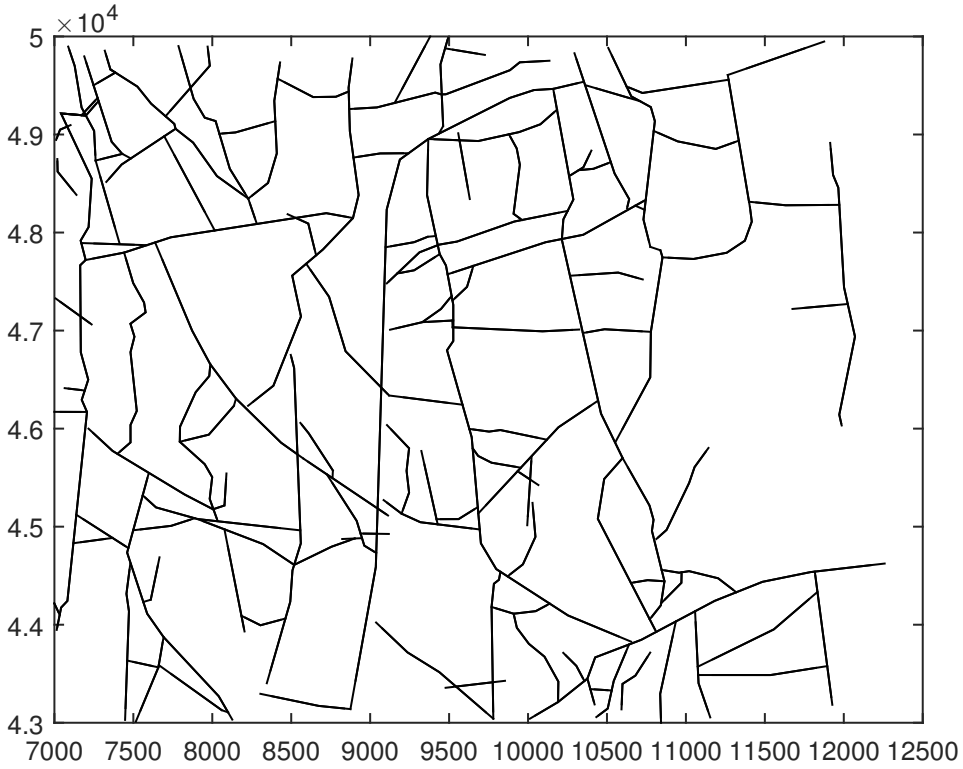

FIGURE 3.9: Complex fracture network

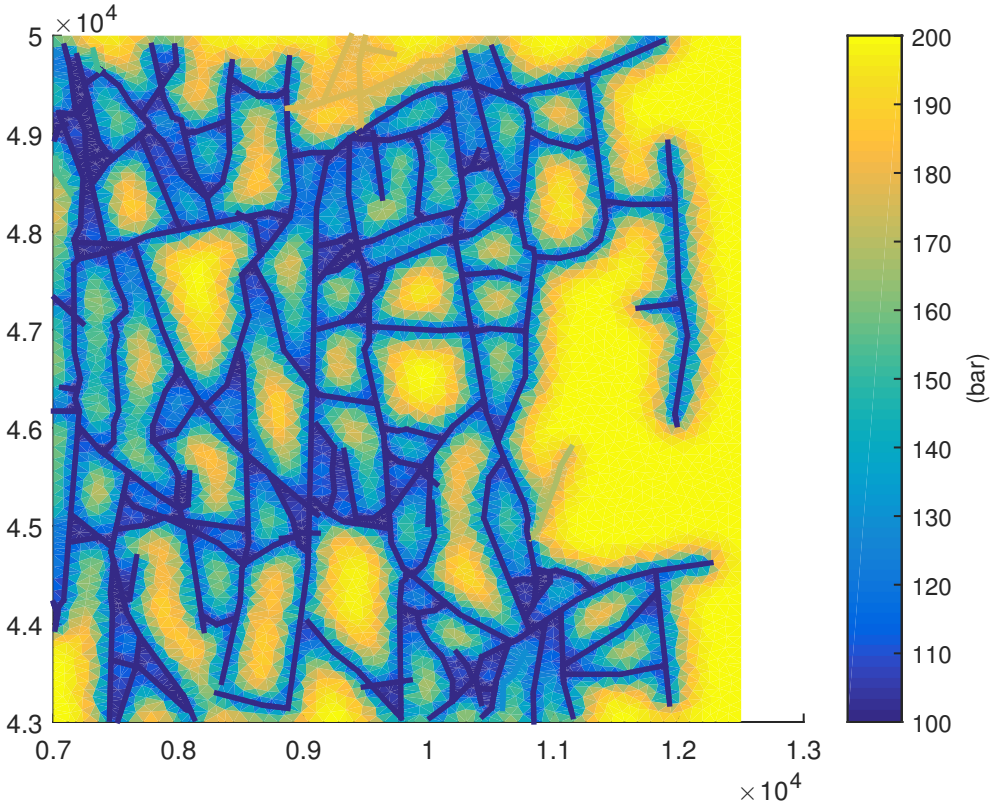

FIGURE 3.10: Flow simulation using shale gas model

Chapter 4

Upscaling

The modelling of large scale and complex fractured reservoir is often computationally demanding, and therefore it is required to use simplified models to improve the efficiency of flow simulations.

Upscaling techniques essentially approximate the static and dynamic characteristics of a fine-scale model into a coarse-scale model, hence it reduces the number of grid blocks for flow simulation.
The simplified models commonly in use in the world of fractured formations, often rely on idealized fracture distribution that doesn't honour the heterogeneity imposed by the actual complex fracture networks.

In this work, we investigate upscaling techniques that take advantage of the detailed fracture models that recent measurements and modelling techniques are able to generate, in order to capture the flow features of fine scale flow simulation in fractured shale gas.

We propose two different methods to achieve that objective, in a procedure that is based on two distinct steps. The first step concerns the building of the coarse grid and the second step is to determine the upscaled transmissibility information from the solution of discrete fracture model as built in the previous chapters.

4.1 First method: Embedded discrete fractures upscaling

The upscaling approach developed here is inspired from the work of Li and Lee (2008), where they propose an embedded fracture modelling (EDFM) technique.
Based on their approach, the matrix domain is discretized separately with a structured Cartesian grid, while the fractures intersecting these matrix blocks are discretized by the matrix cell boundaries, Fig.4.1. The coupling of these two domain was made through a connectivity index based on the concept of the well bore productivity index (PI). In their work they prescribe an analytical approach to approximate this index.

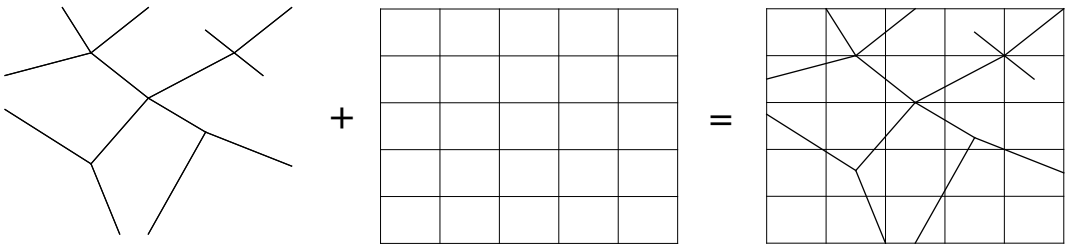

FIGURE 4.1: Discreization of matix domain using a cartesian grid, while fracture are discretized by the matrix cell boundaries in EDFM

In our study, we follow the similar matrix discretisation technique and we apply it for a coarse scale model. At the same time, we define connectivity between the two domains in a different way.

To take advantage of the DFM accuracy in defining the matrix-fracture connectivity, we determine the transmissibility between these two systems in the coarse scale using a fine scale flow simulation from DFM solution.

In general terms, transmissibility expresses the block to block mass flow rate in terms of the difference in pressure between the two blocks.

$$T^k_{i,j} = \frac{\mu}{\rho} \frac{Q^k_{i,j}}{(\overline{p}^k_i - \overline{p}^k_j)} \tag{4.1}$$

From the solution of the fine-scale DFM, we have matrix pressure $\overline{p}^k_i$ and fracture pressure $\overline{p}^k_j$ corresponding to each block k and the flow rate between them $Q^k_{i,j}$. For pressures this is accomplished using a pore volume weighted average of the pressures within the fine scale cells associated with block k, Fig.4.2.

$$\overline{p}^k_i = \frac{\sum_{i \in k} v_i \phi_i p_i}{\sum_{i \in k} v_i \phi_i} \tag{4.2}$$

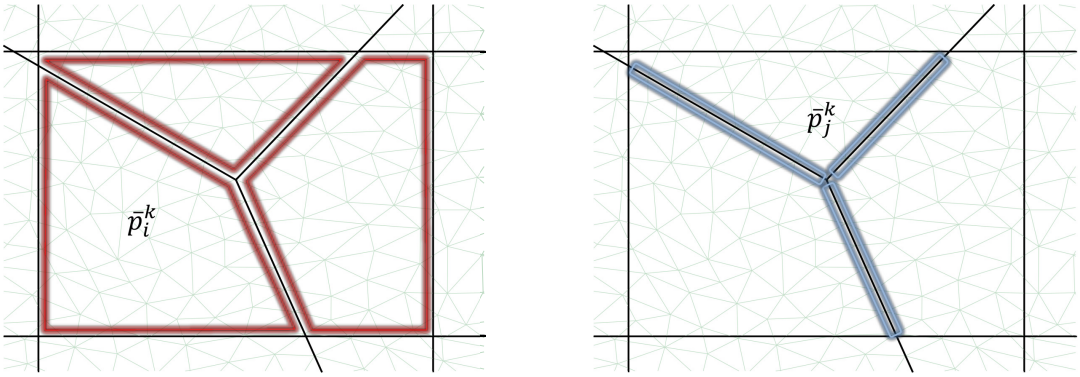

(A) (B)

FIGURE 4.2: Example coarse block k with DFM fine scale unstructured cells in the background (A) represents the fine scale cells from which the average matrix pressure of the coarse scale are calculated (B) fine scale fracture cells used to caluclate average fracture pressure in the coarse scale

The mass flow rate $Q_{i,j}$ is determined from the sum of fluxes crossing the fractures interface within the coarse block k as shown in Fig.4.3.
Matrix-matrix and fracture-fracture transmissibility for the coarse scale are computed in the exact same way used for DFM (Chapter 3) with the only difference that we are using a Cartesian grid to represent the matrix.

Note that we are considering a homogeneous matrix and therefore we do not deal with permeability upscaling in our work.

4.1.1 EDFM Upscaling example cases

In this section we present some application of the described upscaling technique, on a nano-Darcy permeability shale gas problem and on a relatively higher matrix permeability using Darcy formulation. Both problems are tested on the example

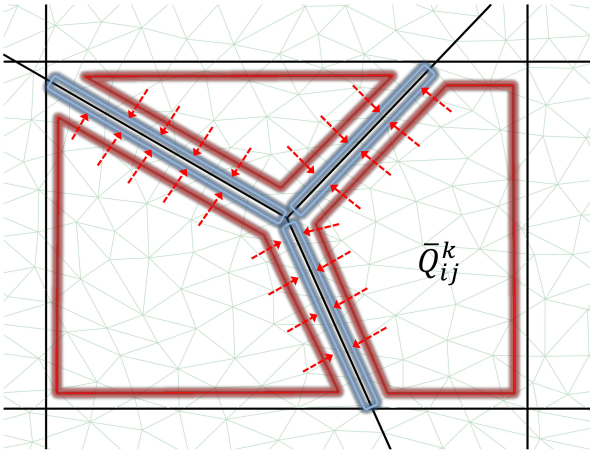

FIGURE 4.3: Mass flux Q_{ij} through the matrix-fracture interface computed from the fine scale DFM solution

fracture distribution previously introduced in chapter 3 in Fig.3.5 with the common properties summarized in table 4.1.

TABLE 4.1: Example fracture system common properties for test cases

Matrix porosity ϕ (%)	6
Fracture aperture (mm)	1
Reservoir temperature $^{\circ}F$	300
Gas viscosity μ (cp)	0.01
Reservoir initial pressure (bar)	200
Producing well BHP (bar)	100

Test Case: Nano-Darcy Shale gas upscaling using method-1

We start by setting up the coarse grid (5 x 5), as shown in Fig. 4.1.
Then to extract the matrix-fracture connectivity information, we run a DFM simulation on a fine scale problem, we use the same fine scale unstructured grid presented in chapter 3 Fig. 3.6.

The simulation consist of a drainage problem, by placing a producing well with constant bottom-hole pressure (bhp) at a point within the connected fracture network. Since the system is isolated due to the no-flow boundaries, the pressure of the domain will get depleted with time and, after a transient period, will reach a pseudo-steady state.
Fig. 4.4 depicts an example plot of the matrix-fracture transmissibility over time for a specific coarse block, indicating the pseudo-steady state at which the upscaled transmissibility is recorded.

Once all the matrix-fracture connections are formulated as well as the rest of the transmissibilities between each of these domains computed, we can now run an upscaled simulation with less number of grid block.
Figure 4.6 shows the results of the upscaled simulation and the fine scale DFM solution at the same time (1000 days), the DFM solution is averaged over the coarse grid block and taken as the reference solution.

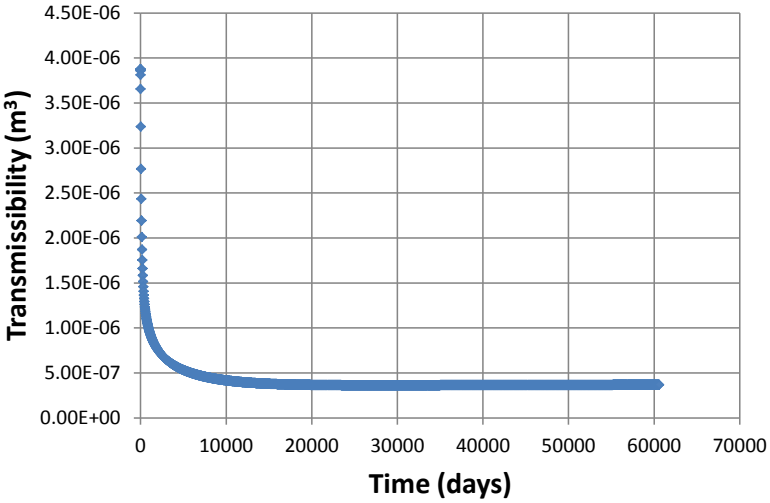

FIGURE 4.4: Matrix-fracture transmissibility plot over time extracted for a specific coarse grid-block.

Notice that transmissibility in general Darcy form is only expressed as a geometrical factor while in the equations derived to emulate shale gas dynamics, transmissibility is pressure dependent.

In our first upscaling attempts we used a constant transmissibility factor, which is representative of the pseudo-steady state regime. The solution obtained has a practical aspect but is not the most accurate.

To improve our results, we introduced a modification to account for the prevailing transient effects in low permeability shale gas. Basically, we decided to fit a linear relationship for the same transmissibility extrated before and consider it as a function of the upwinding pressure as shown in Fig.4.5. This step represent a crucial upgrade to the accuracy of the presented upscaling technique specifically for nano-scale permeabilities.

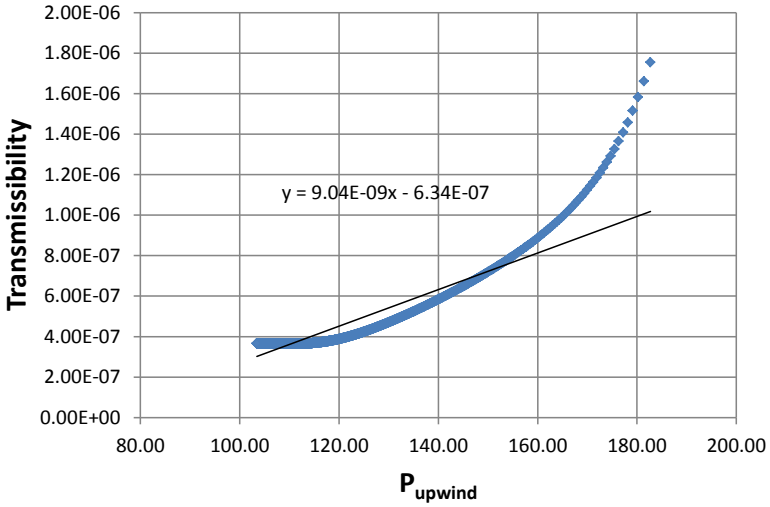

FIGURE 4.5: Transmissibility plotted as a function of upwinded pressure.

The results of the upscaling using an upscaled transmissibility, formulated in terms of the upwinded pressure are shown in Fig.4.7.

Test Case: Upscaling using method-1 for relatively higher k formation

The same procedure is repeated here, for a formation characterized with matrix permeability corresponding to pore size $10^{-8}m$.
The results of the upscaling using the constant pseudo-steady transmissibility are shown in Fig.4.8 and clearly infers that when viscous flow is the dominant transport mechanism, the upscaling techinque explained here provides acceptable resutls.

Table 4.2 and 4.3, summarizes the performance and the accuracy of the embeded fracture upscaling technique on tested examples.

TABLE 4.2: Summary of the performance and accuracy for the shale gas upscaling (test case 1) using method-1

	Total Simulation Time (seconds)	**L2 Pressure Error (%)**
Time steps (days)	**1000**	**1000**
DFM fine scale	30.4	-
EDFM upscale (Trans = const)	2.26	8.5
EDFM upscale (Trans(P))	3.89	5.9

TABLE 4.3: Summary of the performance and accuracy for the higher permeability formation (test case 2) using method-1

	Total Simulation Time (seconds)	**L2 Pressure Error (%)**
Time steps (days)	**150**	**150**
DFM fine scale	13.26	-
EDFM upscale (Trans = const)	0.956	6.7

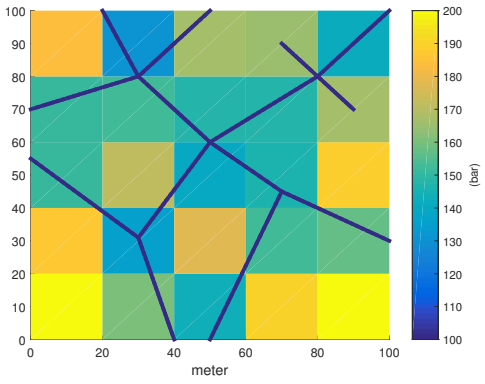

(A) DFM Average

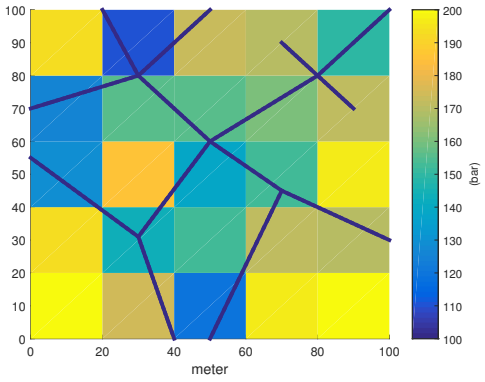

(B) Upscaled solution

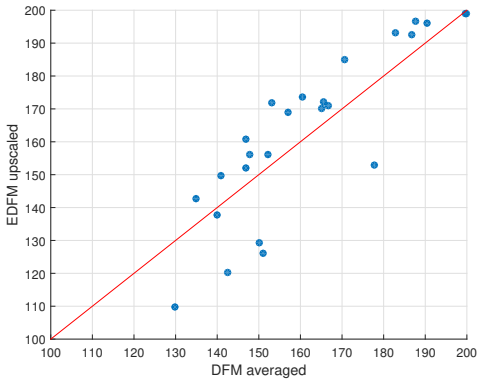

(C)

FIGURE 4.6: Comparison between the upscaled solution (A) and the fine scale averaged solution (B), and the error plot(C) at t = 1000 day

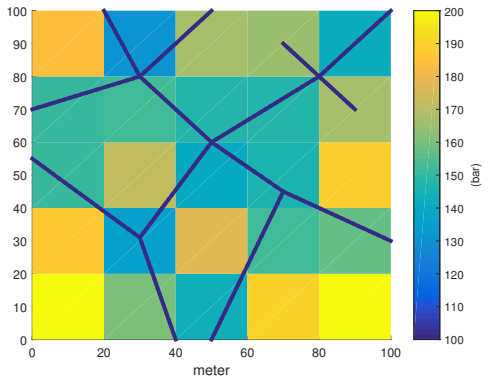

(A) DFM Average

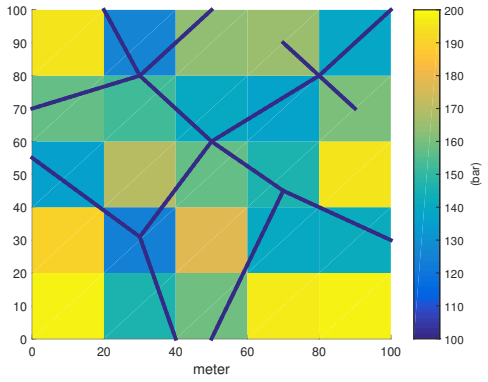

(B) Upscaled solution

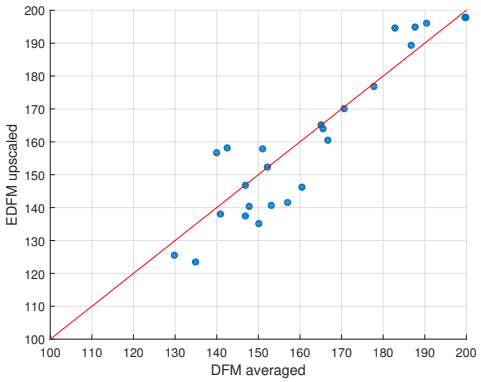

(C)

FIGURE 4.7: Comparison between the upscaled solution using the upgraded transmissibility in terms of upwinded pressure (A) and the fine scale averaged solution (B), and the error plot(C) at t = 1000 day

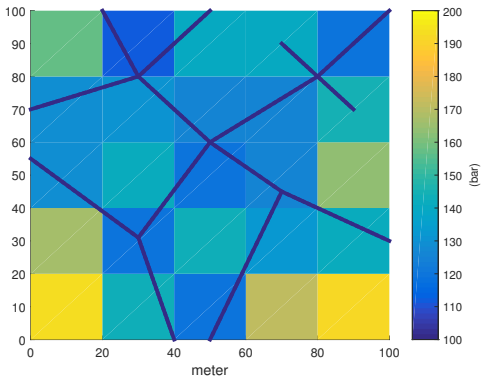

(A) DFM Average

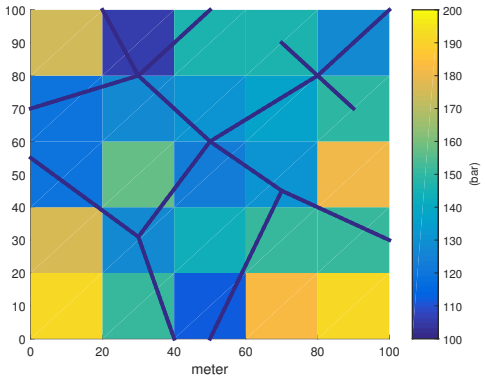

(B) Upscaled solution

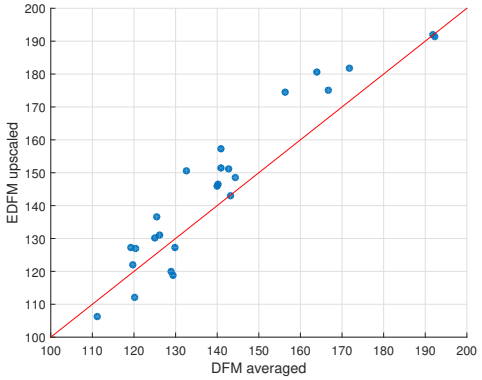

(C)

FIGURE 4.8: Comparison between the upscaled solution for a relatively higher permeability formation (A) and the fine scale averaged solution (B), and the error plot(C) at t = 150 day

4.2 Second method: Multiple subregion (MSR) upscaling

Although acceptable results were obtained from the upscaling procedure described in the previous section, it is remarked that an improvement can be obtained by increasing grid block resolution in the coarse scale. Yet, the use of large Cartesian blocks, for functionality, had masked the flow dynamics and features observed in fine scale flow solution of fractured shale gas. Therefore, we propose another upscaling technique to confront the problem and account for the extended transient effects prevalent in tight formations.

The proposed method suggests the use of a flow based gridding technique to capture the spatial variability within the matrix in a similar way as done in the work of Karimi-Fard et al. (2006).
Based on the fact that pressure variation inside the matrix behaves like a diffusion process, the matrix is divided into regions using iso-pressure curves obtained from the pressure solution of a discrete fracture model.

As in the previous upscaling technique, we obtain the solution of the fine scale model using the formulations derived in the previous chapters. We use this pressure solution for the construction of the multiple subregion model as shown in Fig.4.9, the shapes of the iso-pressure curves are strongly dependent on the fracture geometries as seen. Note that the pressure inside the fractures are approximately the same due to their high permeability.

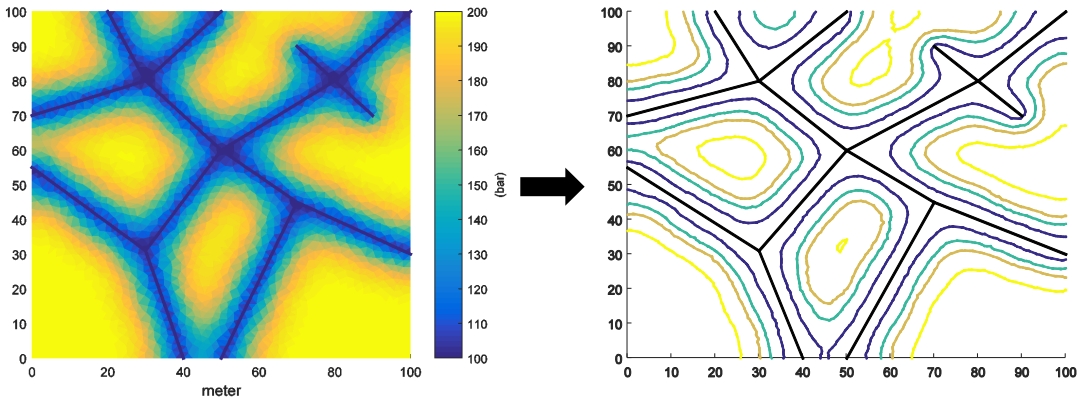

FIGURE 4.9: Iso pressure curves are extracted from the solution of the fine scale DFM to define the coarse scale regions.

The number of subregions in the upscaled model depends on the pressure levels selected, from the DFM solution, to be represented by iso-pressure curves. Fig.4.10 depicts various matrix discretization using iso-pressure curves obtained from the same DFM run, of which the user is free to select depending on the objectives of study.

Once the coarse grid geometry is defined, the next step entails the determination of the connectivity map that will be used for our coarse scale simulation. Fig.4.11 shows a sample of the upscaled domain, indicating that the setup of these regions implies a one dimensional character which allows the representation of the connections using a linear sequence as shown.

We simulate the coarse scale using a finite volume scheme similarly to the previous upscaling technique. Therefore we need to determine the upscaled transmissibility to describe the exchange of flux from one subregion to another or into a

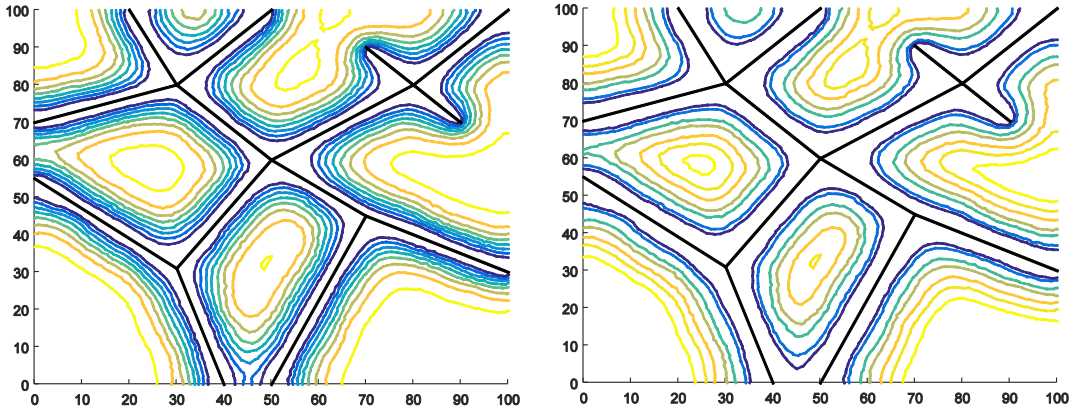

FIGURE 4.10: The number of regions can be varied and selected in different combinations depending on the variation of pressure or the dynamics of pressure diffusion we wish to capture.

fracture. The transmissibility is then defined by

$$T_{i,j} = \frac{\mu}{\rho} \frac{Q_{i,j}}{(\overline{p}_i - \overline{p}_j)} \tag{4.3}$$

The average pressure of each adjacent region and the flux across the interface is also captured from the fine scale DFM simulation as explained in the previous technique.
The use of an upscaled transmissibility linearly associated to the upwinded pressure is also advised to obtain accurate results as shown in the previous technique, especially for formation with a permeability in nanoscale.

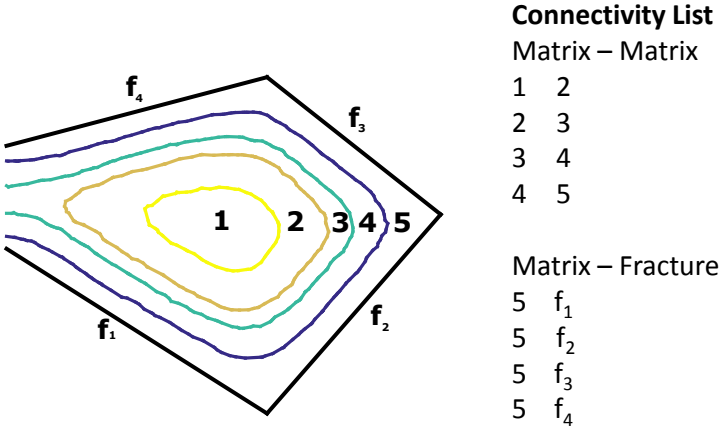

FIGURE 4.11: The construction of the regions imposes a one dimensional scheme for the connectivity list to define the exchange of flow between the regions and fracture.

4.2.1 MSR upscaling example cases

The MSR upscaling results will be illustrated using the example fracture distribution we used so far for most of our test cases as shown in Fig.3.5. The properties of the system are also similar except for the matrix permeability which varies depending on the test case we are analysing.

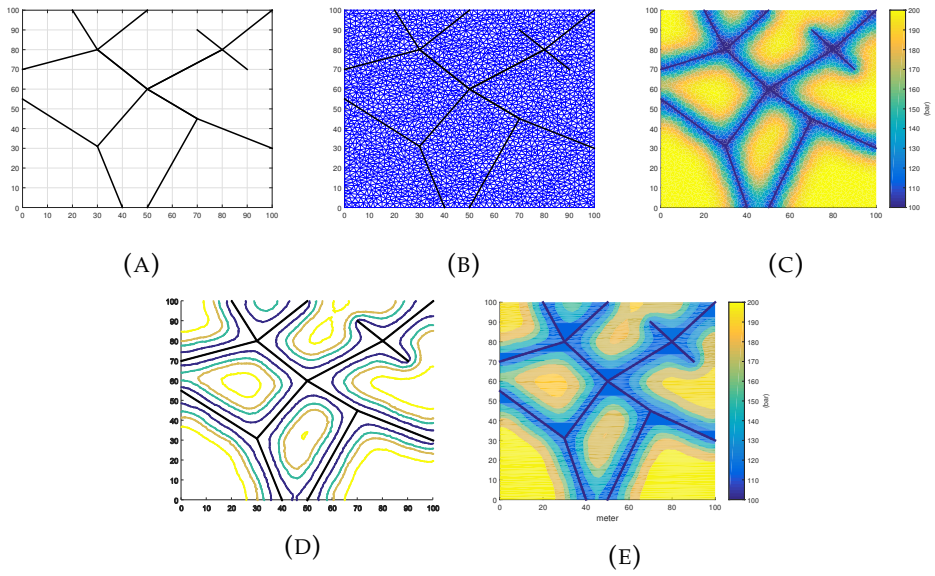

FIGURE 4.12: MSR upscaling workflow sequence

Test Case 1: MSR upscaling of Shale Gas dynamics

Fig.4.12 depicts the workflow in a sequential representation. Starting by the synthetic fracture system composed of 15 fracture segments (all connected) (fig.4.12a), which is then discretized using an unstructured gird into 5223 triangular matrix element for the DFM simulation (fig.4.12b). The model is then simulated for a relatively short period of time (about 1000 day) in order to extract the regions (fig.4.12c). We use 4 pressure levels to generate 41 region in total (fig.4.12d). The next step entails the extraction of the transmissibilities to represent the matrix-matrix and matrix-fracture exchange, to do so we run the DFM model for about 80,000 day (to make sure that pseudo-steady state is reached). Finally, we perform upscaled simulation as in fig.4.12e.

To examine the accuracy of the upscaled solution we compare the results of the upscaling to the fine scale DFM simulations averaged over the coarser cells (regions). Fig.4.13 shows the results of the upscaling solution using the constant pseudo-steady state transmissibility at two different time steps compared to the DFM solution.
We also perform the upscaling using transmissibility taken as a function of the upwinded pressure and we compare it again to the fine scale solution as in Fig.4.14.

Test Case 2: MSR upscaling of low permeability formation using Darcy formulation

We now consider the case of simulating nano-scale permeability formation while neglecting the transport mechanisms attributed to shale gas and only considering viscous flow. As for the rest of properties, the same exact values are used here as in the previous example.

Because we are neglecting slippage effect and the diffusion processes to define the transport of fluid within the formation, we run our simulations for a longer period of time to obtain similar pressure profile as obtained in the previous test case.
We only carry out the upscaling using the constant pseudo-steady state transmissibility, since the results were accurate enough and did not require the use of a pressure dependent transmissibility as shown in Fig.4.15.

TABLE 4.4: MSR upscaling test case 1 (Shale gas dynamics) performance and accuracy summary.

	Total Simulation Time (seconds)		L2 Pressure Error (%)	
Time Steps (days)	**1000**	**5000**	**1000**	**5000**
DFM fine scale	30.4	92.5	-	-
MSR upscale (Trans = const)	1.88	6.32	6.5	6.5
MSR upscale (Trans(P))	3.88	10.78	2.8	2.5

TABLE 4.5: MSR upscaling test case 2 (Darcy) performance and accuracy summary.

	Total Simulation Time (seconds)		L2 Pressure Error (%)	
Time Steps (days)	**5000**	**25000**	**5000**	**25000**
DFM fine scale	47.4	176.3	-	-
MSR upscale (Trans = const)	6.61	24.76	2.7	2.1

Table 4.4 and 4.5 summarizes the performance and accuracy of the MSR upscaling technique in the presented examples.

4.3 Discussion

In this chapter we presented a systematic methodology for constructing two different upscaling models from detailed fracture characterization. From the analysis of the L2 error, summarized in tables (4.2,4.3,4.4, and 4.5), we notice that the upscaling results from the MSR method, using flow based coarse grid, is probably more accurate in capturing the flow features observed in the DFM fine scale solution. However, the EDFM upscaling method, using Cartesian coarse grids, provides an easier workflow whose accuracy depends on the resolution of the coarse grids, additional results with higher resolution are presented in the appendix A. We also notice that the upscaling of shale gas dynamics, requires the use of a pressure dependent upscaled transmissibility to obtain more accurate results, while the upscaling of viscous dominated flow using a constant pseudo-steady state transmissibility is considered sufficiently enough to obtain acceptable results.

The EDFM upscaling procedure can be furtherly optimized by restricting the DFM model and fine scale grid only to the coarse blocks intersected by fracture segments rather than solving the DFM problem over the whole domain.

In the original MSR upscaling work, the subregions were defined using the pseudo-steady state DFM solution. We realize that the regions can be created, first of all, using the DFM solution of problems formulated with simpler physics such as Darcy formulation rather than shale gas formulation as long as the pressure diffusion dynamics are captured. This also implies that the DFM solution does not necessarily need to be captured at pseudo-steady state as long as the proper pressure levels to be represented are selected as we've shown in Fig.4.10. On the other hand, the higher the resolution of the DFM solution, from which the flow based coarse grids are built, the sharper and better will be the regions outcome.

The effect of the DFM grid resolution on the upscaled transmissibility calculation was examined in this work; we present MSR upscaled results based on a lower resolution DFM solution summarized in appendix A, a quick look at the results suggests that the accuracy is not strongly impacted by the reduced resolution.

The application of the proposed upscaling approaches on the detailed fractured characterization obtained from Boersma (2016) is represented in appendix B along with the results summary.

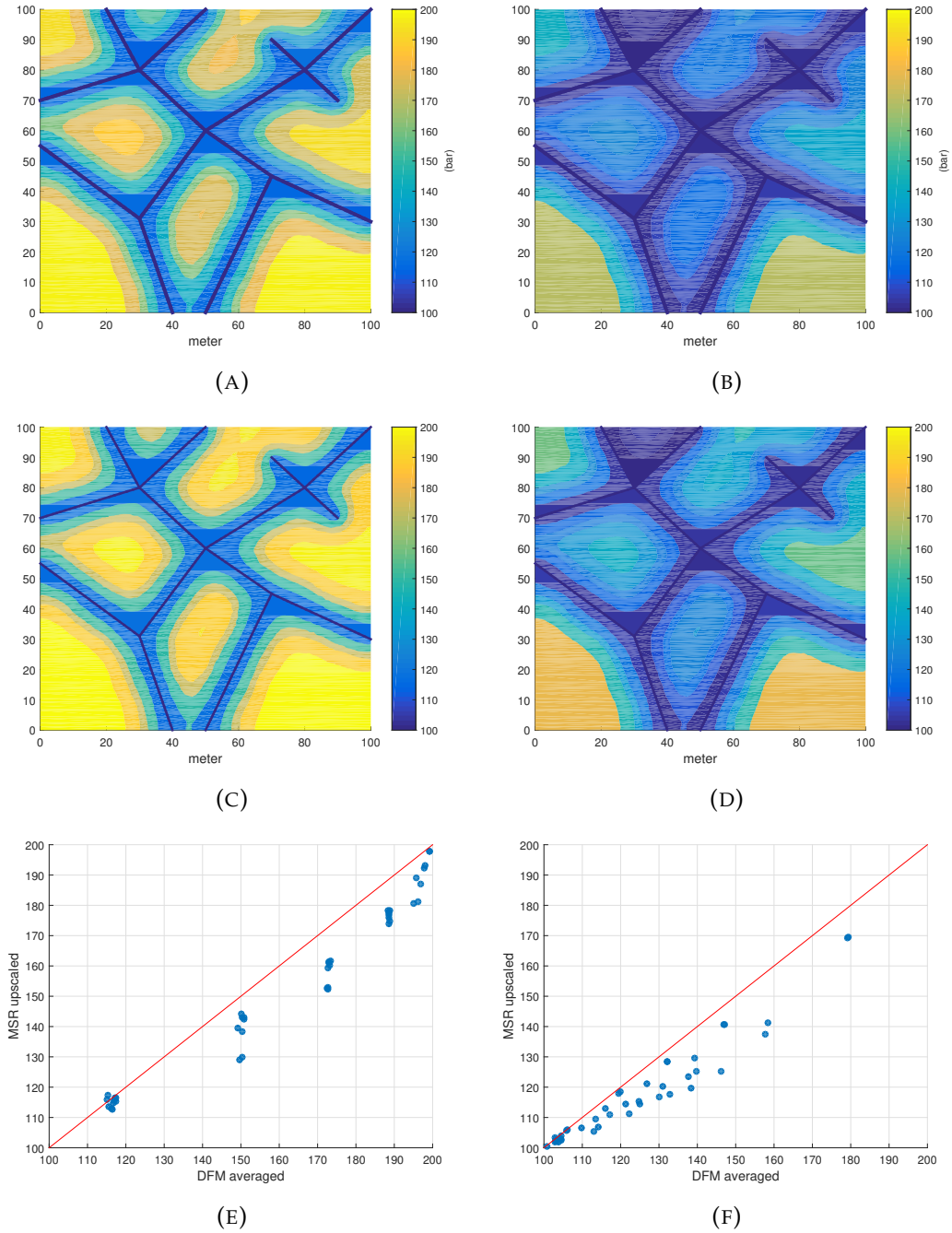

FIGURE 4.13: MSR upscaling results of shale gas dynamics using constant transmissibility, on the left side the results correspond to 1000 days of production and on the right side the results for the 5000 days simulation. (A) & (B) represents the upscaling results, (C) & (D) are the DFM averaged results,and (E) & (F) is a comparison of the upscaled results to the fine scale ones.

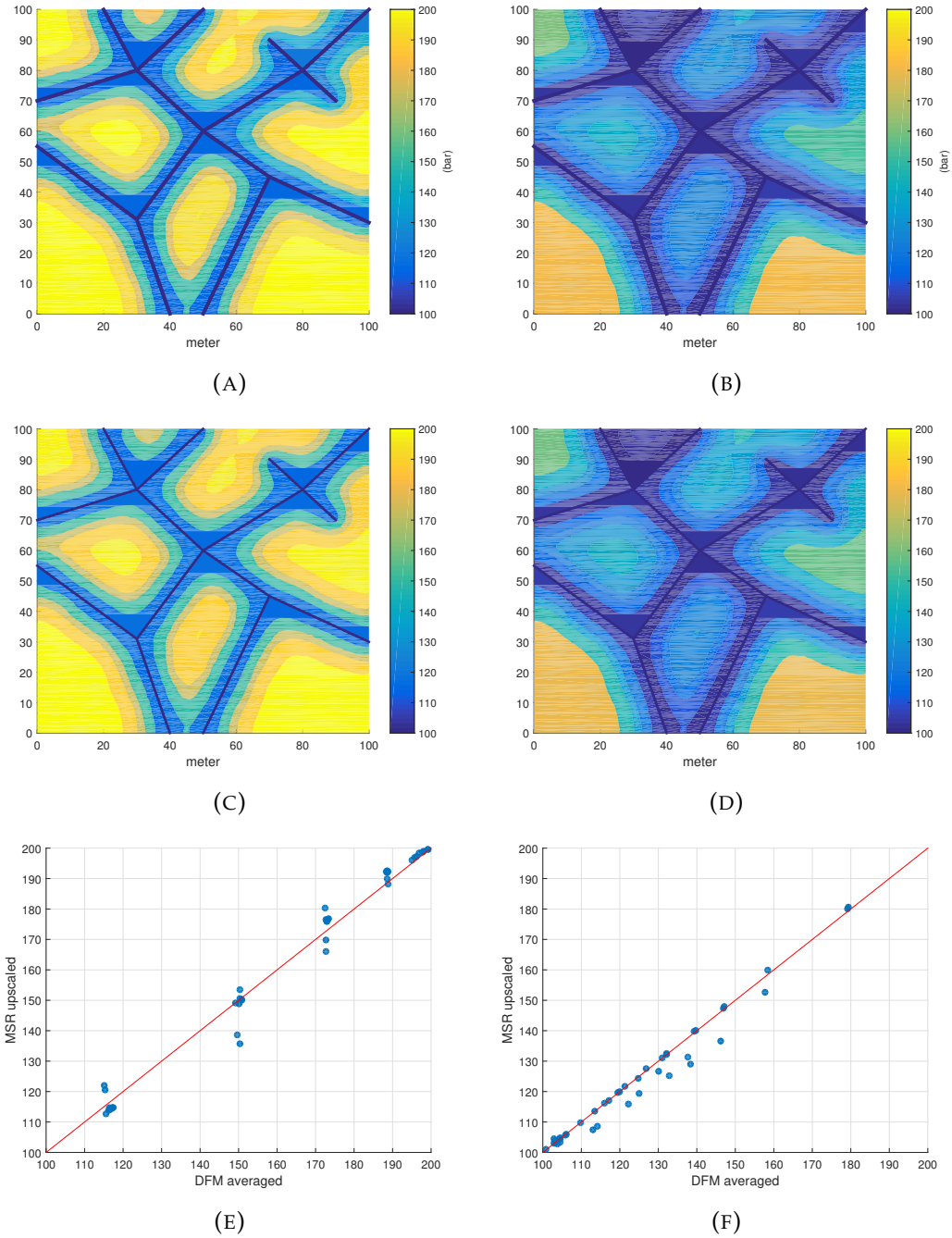

FIGURE 4.14: MSR upscaling results of shale gas dynamics using pressure dependent transmissibility, on the left side the results correspond to 1000 days of production and on the right side the results for the 5000 days simulation. (A) & (B) represents the upscaling results, (C) & (D) are the DFM averaged results,and (E) & (F) is a comparison of the upscaled results to the fine scale ones.

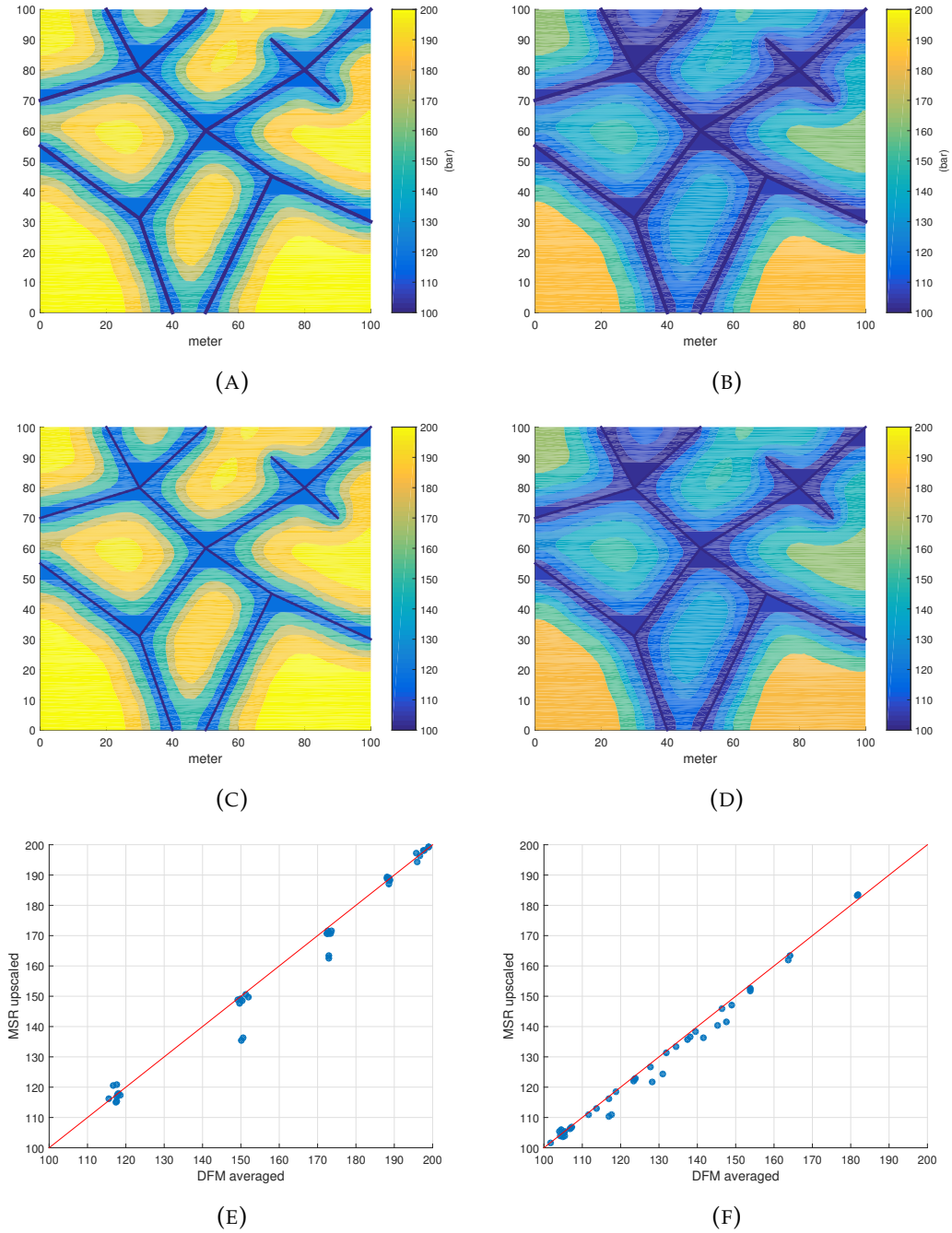

FIGURE 4.15: MSR upscaling results for Darcy model in low permeability, on the left side the results correspond to 1000 days of production and on the right side the results for the 5000 days simulation. (A) & (B) represents the upscaling results, (C) & (D) are the DFM averaged results,and (E) & (F) is a comparison of the upscaled results to the fine scale ones.

Chapter 5

Conclusions

In this thesis, shale gas dynamics were investigated and implemented into a DFM approach in order to capture the highly detailed geological features of fractured shale formations. For that we implemented shale gas formulation into the finite volume based discrete fracture model, presented by Karimi-Fard et al. (2003). The technique is meant to handle unstructured grids, for which we have shown the application of a triangulation gridding scheme that has the ability to efficiently discretize complex fractured networks.

The influence of the various transport mechanisms, induced by the low permeability of shale gas, was shown through successful flow simulations examples carried out by the described DFM technique. We obtained these results using the equations of a bundle of dual tubes (Lunati and Lee, 2014), initially derived for a statistical model, which we numerically adapted into a general purpose reservoir simulator using a connection list approach (ADGPRS).

Despite proven to be efficient for simulating flow across complex fracture networks of relatively small scale, performing DFM simulations for large scale shale gas fields wouldn't be practical. Simulations of that size, would involve an extremely large amount of grid cells beyond the computational capabilities or time constraints of reservoir simulators. Hence, the application of upscaling techniques is usually the favorable choice in practice but also causes the dilution of details in heterogeneous environment.

For that reason, we thoroughly investigated and proposed the application of two systematic upscaling technique that honor detailed fracture characterizations and applicable to shale gas. Moreover, these proposed methods are linked to the results of accurate DFM technique as their resource to formulate the upscaling parameters. Our first approach can be seen as an adaptation of the EDFM method, as the coarse scale is made of structured grid blocks and the fractures are embedded within. This method has the advantage of being easier to apply as only the matrix-fracture connections are upscaled from the DFM solution. We then proposed a second upscaling model which uses a flow based gridding technique for the coarse level similarly to the MSR upscaling technique in Karimi-Fard et al. (2006) and Gong et al. (2006). The regions are obtained from the DFM flow simulation which depicts the pressure diffusion character of fractured shale gas under production. Then we extract the upscaling parameters, in that case for matrix-matrix and matrix-fracture connections, similarly to our first approach. Using the flow based regions to form the upscaled blocks offers an improved accuracy in replicating the flowing profile of the DFM solution with a significant reduction in the number of grid cells.

On the other hand, we have shown that to depict the transient character of low permeability shale gas, one need to consider the pressure dependency in the parameters defining the mass transfer across the regions. For that, we correlated the transmissibility to the upwinding pressure and obtained better results that we validated

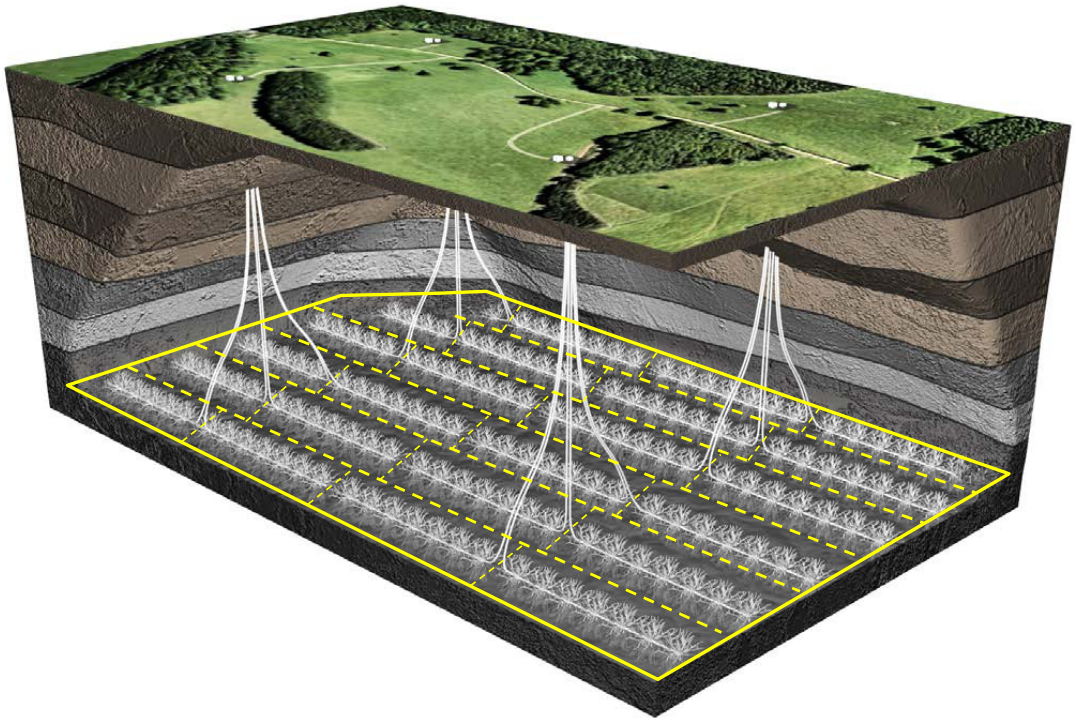

FIGURE 5.1: Shale gas development strategies (Courtesy Statoil)

it by the fine scale DFM solution.

Lastly, we consider our upscaling models to be mostly convenient for shale gas field simulation. As shown in Fig.5.1 shale gas fields can be divided into separate isolated blocks each of which drained by an individual well; as the low permeability of these formation limits to almost none the interference between wells. This aspect allows us to run global DFM flow simulation for each isolated block, and can be considered an achievable objective for determining the upscaled parameters. The use of a global flow solution with no flow boundaries is the key optimization and advantage over many of the available upscaling techniques that rely on local flow problems with specified boundaries to obtain the upscaling parameters, which introduces additional steps and errors.

Appendix A

Influence of Resolution

A.1 EDFM upscaling using higher resolution coarse grid blocks

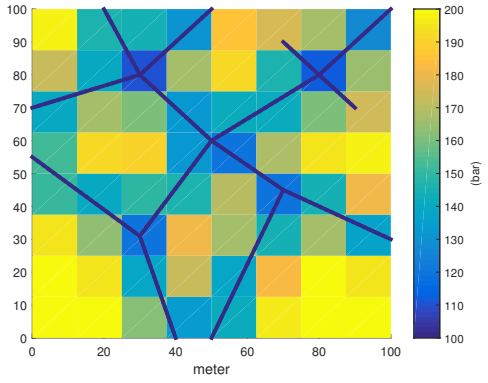

(A) DFM Average

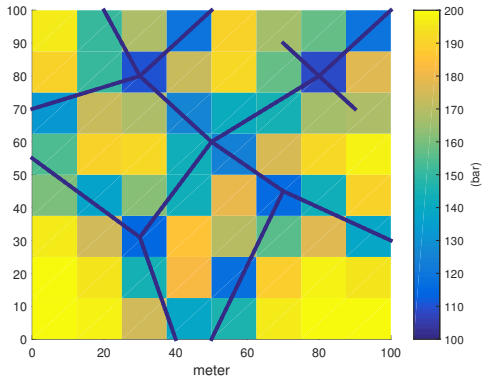

(B) Upscaled solution

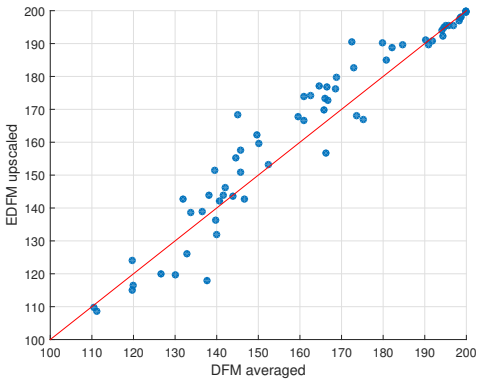

(C)

FIGURE A.1: Comparison between the EDFM upscaled solution using a higher resolution (8x8) coarse grid, shale gas formulation and pseudo-steady state transmissibility (A) and the fine scale averaged solution (B), and the error plot (C) at t = 1000 day

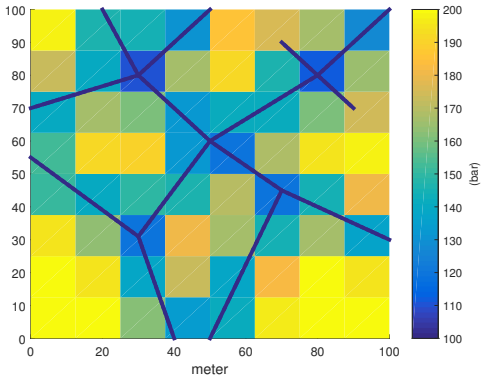

(A) DFM Average

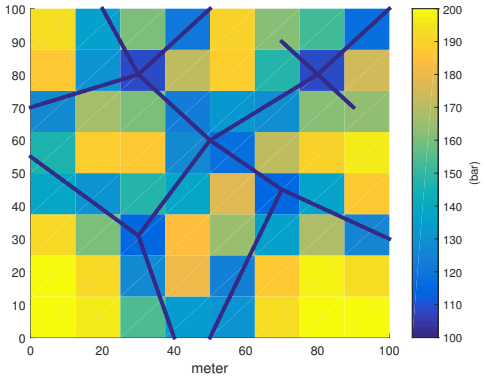

(B) Upscaled solution

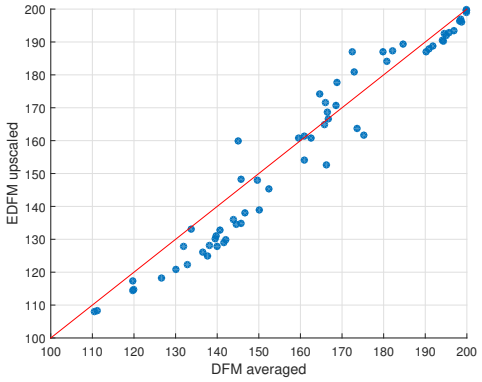

(C)

FIGURE A.2: Comparison between the EDFM upscaled solution using a higher resolution (8x8) coarse grid, shale gas formulation and a pressure dependent transmissibility (A) and the fine scale averaged solution (B), and the error plot (C) at t = 1000 day

TABLE A.1: EDFM upscaling (Shale gas dynamics, high resolution coarse grid) performance and accuracy summary.

	Total Simulation Time (seconds)	**L2 Pressure Error (%)**
Time steps (days)	**1000**	
DFM (5223 triangle)	30.4	-
EDFM upscale (Trans = const)	2.76	5.19
EDFM upscale (Trans (P))	3.27	4.8

A.2 MSR upscaling using lower resolution DFM

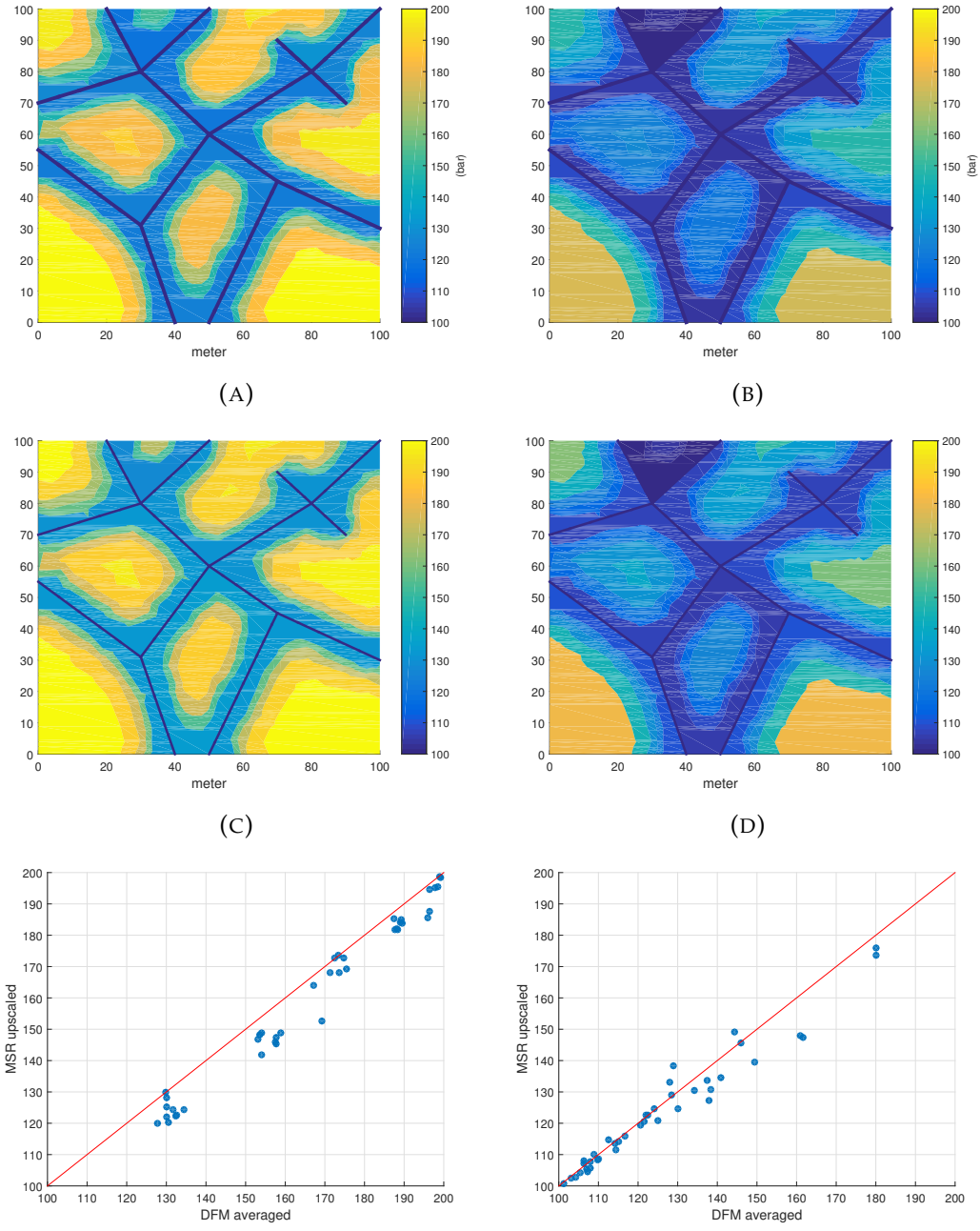

(A) (B)

(C) (D)

(E) (F)

FIGURE A.3: MSR upscaling results of shale gas dynamics using low resolution DFM, constant transmissibility. On the left side the results correspond to 1000 days of production and on the right side the results for the 5000 days simulation. (A) & (B) represents the upscaling results, (C) & (D) are the DFM averaged results,and (E) & (F) is a comparison of the upscaled results to the fine scale ones.

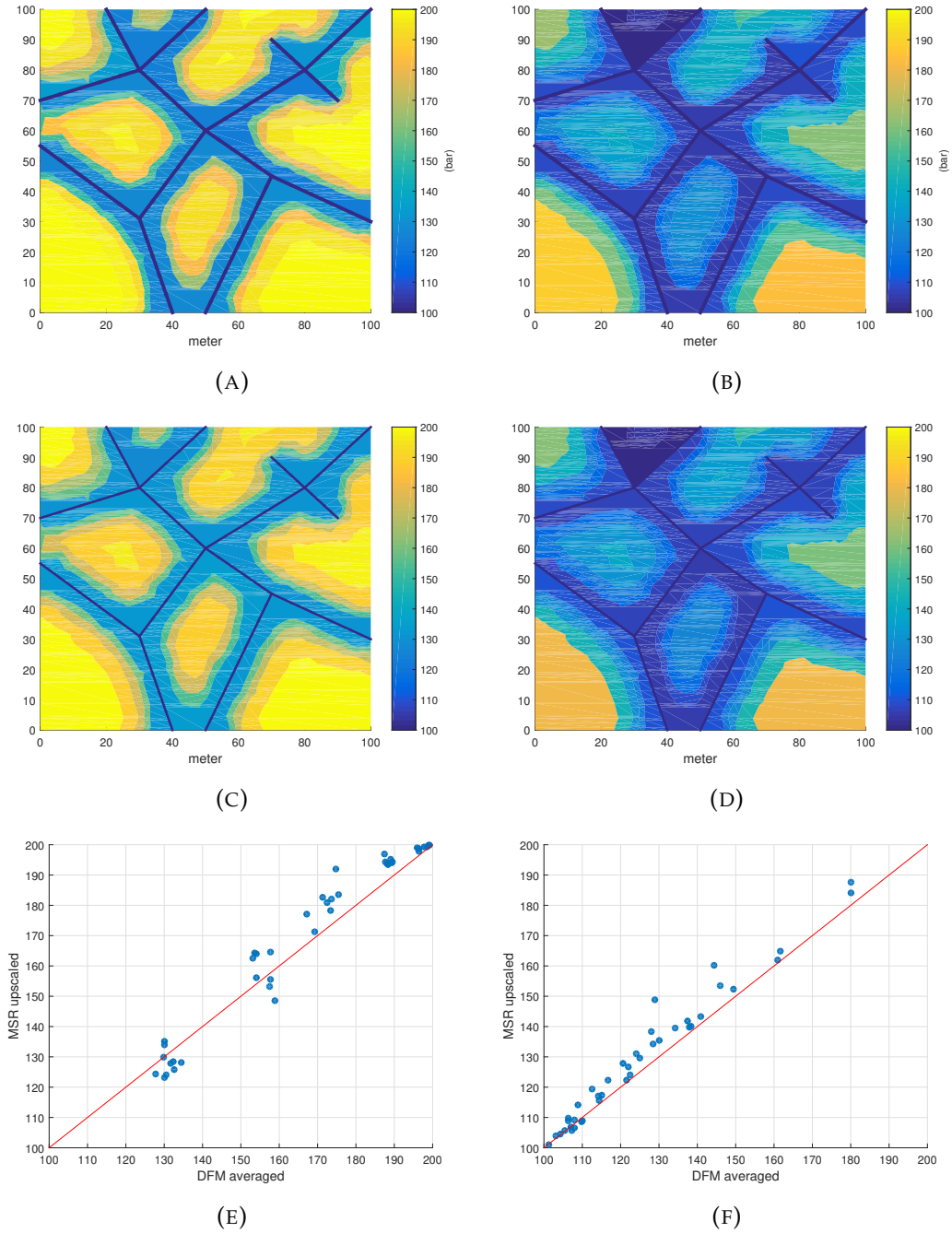

FIGURE A.4: MSR upscaling results of shale gas dynamics using low resolution DFM, pressure dependent transmissibility. On the left side the results correspond to 1000 days of production and on the right side the results for the 5000 days simulation. (A) & (B) represents the upscaling results, (C) & (D) are the DFM averaged results,and (E) & (F) is a comparison of the upscaled results to the fine scale ones.

TABLE A.2: MSR upscaling (Shale gas dynamics, low resolution DFM) performance and accuracy summary.

	Total Simulation Time (seconds)		**L2 Pressure Error (%)**	
Time steps (days)	**1000**	**5000**	**1000**	**5000**
DFM	3.6	10.65	-	-
MSR upscale (Trans = const)	1.13	4.86	4.7	3.46
MSR upscale (Trans (P))	1.54	5.24	4.15	4.38

Appendix B

Large Scale Fracture Network Upscaling

B.1 EDFM upscaling of large scale fracture system

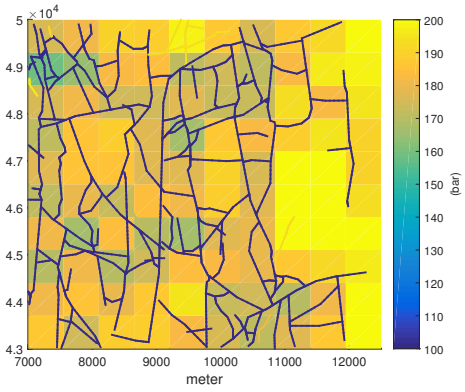

(A) DFM Average

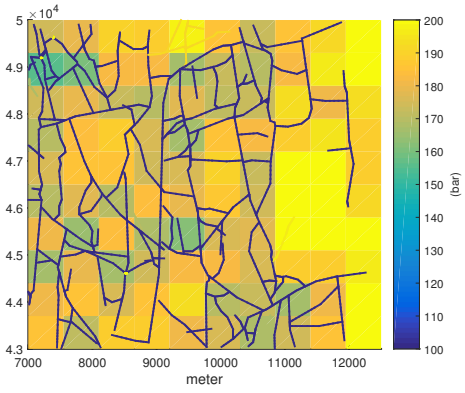

(B) Upscaled solution

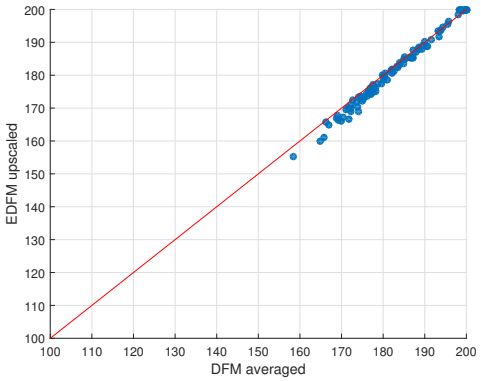

(C)

FIGURE B.1: Comparison between the EDFM upscaled solution for the large scale fracture system (10x10) coarse grid, shale gas formulation and a pressure dependent transmissibility (A) and the fine scale averaged solution (B), and the error plot (C) at t = 10000 day

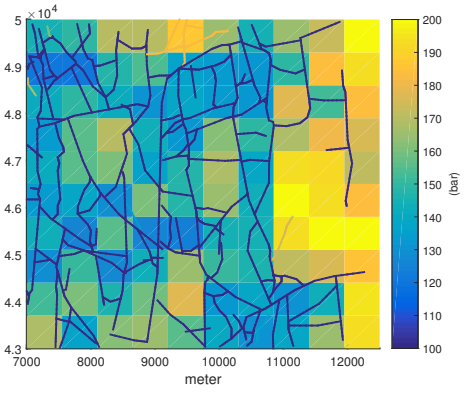

(A) DFM Average

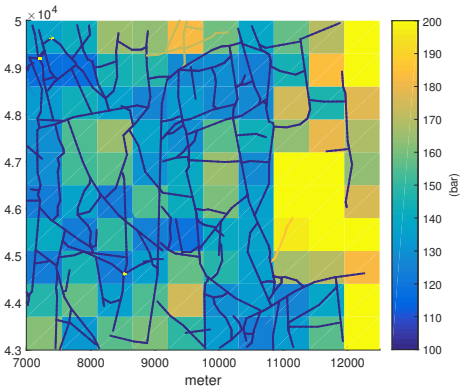

(B) Upscaled solution

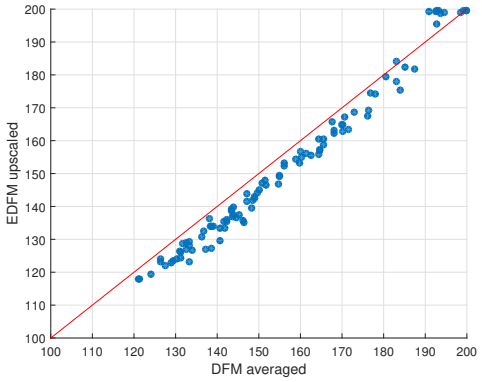

(C)

FIGURE B.2: Comparison between the EDFM upscaled solution for the large scale fracture system (10x10) coarse grid, shale gas formulation and a pressure dependent transmissibility (A) and the fine scale averaged solution (B), and the error plot (C) at t = 50000 day

TABLE B.1: EDFM upscaling (Shale gas dynamics, large scale fracture system) performance and accuracy summary.

	Total Simulation Time (seconds)		**L2 Pressure Error (%)**	
Time steps (days)	**10000**	**50000**	**10000**	**50000**
DFM (15972 triangle)	533	2268	-	-
EDFM upscale (Trans (P))	141.6	662.9	1.04	3.975

B.2 MSR upscaling of large scale fracture system

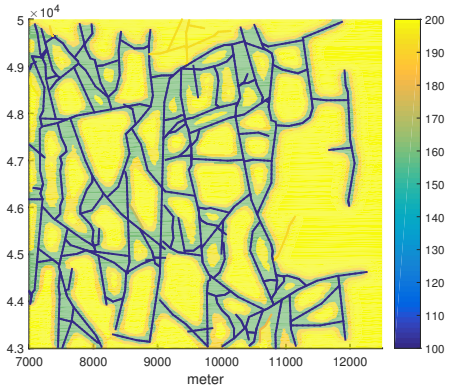

(A) DFM Average

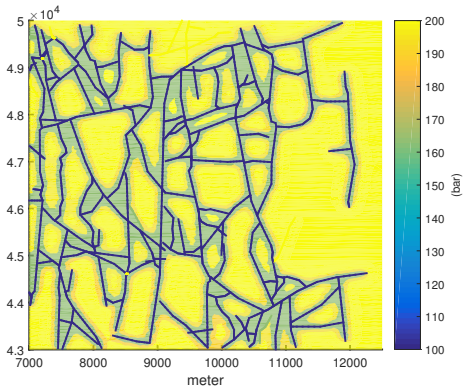

(B) Upscaled solution

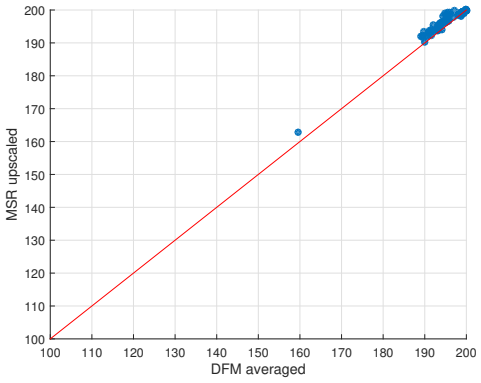

(C)

FIGURE B.3: Comparison between MSR upscaled solution (143 region) for the large scale fracture system (A) using shale gas formulation and a pressure dependent transmissibility, and the fine scale averaged solution (B), and the error plot (C) at t = 10000 day

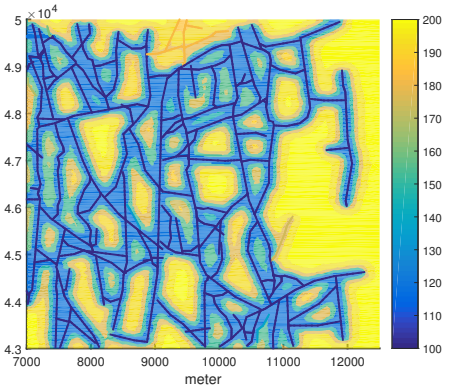

(A) DFM Average

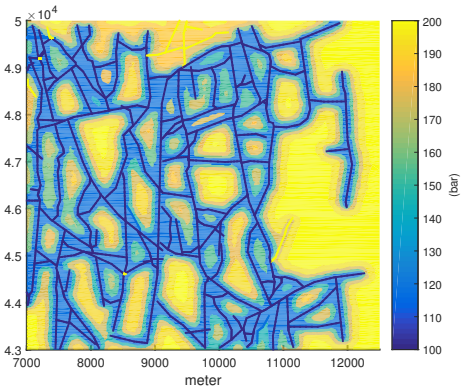

(B) Upscaled solution

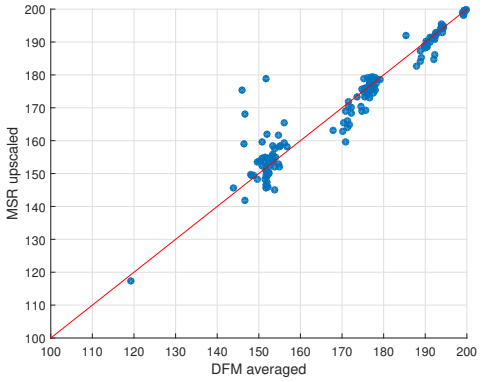

(C)

FIGURE B.4: Comparison between MSR upscaled solution (143 region) for the large scale fracture system (A) using shale gas formulation and a pressure dependent transmissibility, and the fine scale averaged solution (B), and the error plot (C) at t = 50000 day

TABLE B.2: MSR upscaling (Shale gas dynamics, large scale fracture system) performance and accuracy summary.

	Total Simulation Time (seconds)		**L2 Pressure Error (%)**	
Time steps (days)	**10000**	**50000**	**10000**	**50000**
DFM	533	2268	-	-
MSR upscale (Trans (P))	247.5	1178	0.68	3.34

Bibliography

Baca, RG, RC Arnett, and DW Langford (1984). "Modelling fluid flow in fractured-porous rock masses by finite-element techniques". *International Journal for Numerical Methods in Fluids* 4.4, pp. 337–348.

Barenblatt, GI and Yu P Zheltov (1960). "Fundamental equations of filtration of homogeneous liquids in fissured rocks". *Soviet Physics Doklady*. Vol. 5, p. 522.

Berkowitz, Brian (2002). "Characterizing flow and transport in fractured geological media: A review". *Advances in water resources* 25.8, pp. 861–884.

Blaskovich, FT et al. (1983). "A multicomponent isothermal system for efficient reservoir simulation". *Middle East Oil Technical Conference and Exhibition*. Society of Petroleum Engineers.

Blunt, Martin J et al. (2013). "Pore-scale imaging and modelling". *Advances in Water Resources* 51, pp. 197–216.

Boersma, QD (2016). "Horizontal fracture-fault network characterization of pavement imagery of the Whitby Mudstone". MA thesis.

Brown, Gordon P et al. (1946). "The flow of gases in pipes at low pressures". *Journal of Applied Physics* 17.10, pp. 802–813.

Darabi, Hamed et al. (2012). "Gas flow in ultra-tight shale strata". *Journal of Fluid Mechanics* 710.1, pp. 641–658.

Fatt, I (1956). "The network model of porous media III. Dynamic properties of networks with tube radius distribution". *Trans. AIME* 207, pp. 164–181.

Fu, Yao, Y-K Yang, and M Deo (2005). "Three-dimensional, three-phase discrete-fracture reservoir simulator based on control volume finite element (CVFE) formulation". *SPE Reservoir Simulation Symposium*. Society of Petroleum Engineers.

Geiger-Boschung, Sebastian et al. (2009). "Black-oil simulations for three-component, three-phase flow in fractured porous media". *SPE journal* 14.02, pp. 338–354.

Gong, Bin, Mohammad Karimi-Fard, and Louis J Durlofsky (2006). "An upscaling procedure for constructing generalized dual-porosity/dual-permeability models from discrete fracture characterizations". *SPE Annual Technical Conference and Exhibition*. Society of Petroleum Engineers.

Hadjiconstantinou, Nicolas G (2006). "The limits of Navier-Stokes theory and kinetic extensions for describing small-scale gaseous hydrodynamics". *Physics of Fluids (1994-present)* 18.11, p. 111301.

Hill, AC and GW Thomas (1985). "A new approach for simulating complex fractured reservoirs". *Middle East Oil Technical Conference and Exhibition*. Society of Petroleum Engineers.

Hirschfelder, Joseph O et al. (1954). *Molecular theory of gases and liquids*. Vol. 26. Wiley New York.

Hoteit, Hussein and Abbas Firoozabadi (2005). "Multicomponent fluid flow by discontinuous Galerkin and mixed methods in unfractured and fractured media". *Water Resources Research* 41.11.

Javadpour, Farzam, D Fisher, and M Unsworth (2007). "Nanoscale gas flow in shale gas sediments". *Journal of Canadian Petroleum Technology* 46.10.

Juanes, Ruben, Javier Samper, and Jorge Molinero (2002). "A general and efficient formulation of fractures and boundary conditions in the finite element method". *International Journal for Numerical Methods in Engineering* 54.12, pp. 1751–1774.

Karimi-Fard, M (2008). "Grid optimization to improve orthogonality of two-point flux approximation for unstructured 3D fractured reservoirs". *ECMOR XI-11th European Conference on the Mathematics of Oil Recovery*.

Karimi-Fard, Mohammad and Abbas Firoozabadi (2001). "Numerical simulation of water injection in 2D fractured media using discrete-fracture model". *SPE annual technical conference and exhibition*. Society of Petroleum Engineers.

Karimi-Fard, Mohammad, Luis J Durlofsky, and K Aziz (2003). "An efficient discrete fracture model applicable for general purpose reservoir simulators". *SPE Reservoir Simulation Symposium*. Society of Petroleum Engineers.

Karimi-Fard, Mohammad, Bin Gong, and Luis J Durlofsky (2006). "Generation of coarse-scale continuum flow models from detailed fracture characterizations". *Water resources research* 42.10.

Kim, Jong-Gyun and Milind D Deo (2000). "Finite element, discrete-fracture model for multiphase flow in porous media". *AIChE Journal* 46.6, pp. 1120–1130.

Lee, Seong H, MF Lough, and CL Jensen (2001). "Hierarchical modeling of flow in naturally fractured formations with multiple length scales". *Water Resources Research* 37.3, pp. 443–455.

Lee, SH, L Padmanabhan, and HA Al-Sunaidi (1996). "Simulation of linear displacement experiments on massively parallel computers". *SPE Journal* 1.03, pp. 327–340.

Li, Liyong and Seong H Lee (2008). "Efficient field-scale simulation of black oil in a naturally fractured reservoir through discrete fracture networks and homogenized media". *SPE Reservoir Evaluation & Engineering* 11.04, pp. 750–758.

Lunati, I and SH Lee (2014). "A dual-tube model for gas dynamics in fractured nanoporous shale formations". *Journal of Fluid Mechanics* 757, pp. 943–971.

Matthäi, SK, A Mezentsev, M Belayneh, et al. (2005). "Control-volume finite-element two-phase flow experiments with fractured rock represented by unstructured 3D hybrid meshes". *SPE Reservoir Simulation Symposium*. Society of Petroleum Engineers.

Matthäi, SK et al. (2007). "Numerical simulation of multi-phase fluid flow in structurally complex reservoirs". *Geological Society, London, Special Publications* 292.1, pp. 405–429.

Ponting, David K (1989). "Corner point geometry in reservoir simulation". *ECMOR I-1st European Conference on the Mathematics of Oil Recovery*.

Sablok, R and K Aziz (2008). "Upscaling and discretization errors in reservoir simulation". *Petroleum Science and Technology* 26.10-11, pp. 1161–1186.

Sarkar, Sudipta, M Nafi Toksoz, and Daniel R Burns (2004). *Fluid flow modeling in fractures*. Tech. rep. Massachusetts Institute of Technology. Earth Resources Laboratory.

Shewchuk, Jonathan Richard (1996). "Triangle: Engineering a 2D quality mesh generator and Delaunay triangulator". *Applied computational geometry towards geometric engineering*. Springer, pp. 203–222.

Vitel, Sarah and Laurent Souche (2007). "Unstructured upgridding and transmissibility upscaling for preferential flow paths in 3D fractured reservoirs". *SPE Reservoir Simulation Symposium*. Society of Petroleum Engineers.

Voskov, Denis (2012). "An extended natural variable formulation for compositional simulation based on tie-line parameterization". *Transport in porous media* 92.3, pp. 541–557.

Voskov, Denis Viktorovich and Hamdi A Tchelepi (2011). "Compositional nonlinear solver based on trust regions of the flux function along key tie-lines". *SPE Reservoir Simulation Symposium*. Society of Petroleum Engineers.

Voskov, Denis Viktorovich, Hamdi A Tchelepi, and Rami Younis (2009). "General nonlinear solution strategies for multiphase multicomponent eos based simulation". *SPE Reservoir Simulation Symposium*. Society of Petroleum Engineers.

Warren, JE and P Jj Root (1963). "The behavior of naturally fractured reservoirs". *Society of Petroleum Engineers Journal* 3.03, pp. 245–255.

Yang, Tingyun, Xiang Li, and Dongxiao Zhang (2015). "Quantitative dynamic analysis of gas desorption contribution to production in shale gas reservoirs". *Journal of Unconventional Oil and Gas Resources* 9, pp. 18–30.

Yu, Wei and Kamy Sepehrnoori (2014). "Simulation of gas desorption and geomechanics effects for unconventional gas reservoirs". *Fuel* 116, pp. 455–464.

Zaydullin, Rustem, Denis Voskov, and Hamdi A Tchelepi (2012). "Nonlinear formulation based on an equation-of-state free method for compositional flow simulation". *SPE Journal* 18.02, pp. 264–273.

Zhou, Yifan, Hamdi A Tchelepi, and Bradley T Mallison (2011). "Automatic differentiation framework for compositional simulation on unstructured grids with multi-point discretization schemes". *SPE Reservoir Simulation Symposium*. Society of Petroleum Engineers.